Beta Oscillations in Frontal Cortex and Striatum Represent Post-Processing of Successful Behavior

by

Joseph Feingold

AB Philosophy and Physics
Harvard University, 1999
Master of Advanced Study in Mathematics
Cambridge University, 2000

Submitted to the Division of Health Sciences and Technology
in Partial Fulfillment of the Requirements for the Degree of

Doctor of Philosophy in Health Sciences and Technology

at the

Massachusetts Institute of Technology

September 2011

Signature of Author: _____
Speech and Hearing Bioscience and Technology Program
September 1, 2011

Certified by: _____
Ann M. Graybiel, PhD
Institute Professor and Professor in Brain and Cognitive Sciences
Thesis Supervisor

Accepted by: _____
Ram Sasisekharan, PhD
Director, Harvard-MIT Division of Health Sciences and Technology
Edward Hood Taplin Professor of Health Sciences & Technology and Biological Engineering

ACKNOWLEDGEMENTS

Thank you to my wife, Shiri, and to my parents and family, friends and colleagues.

כִּי בְּרֹב חָכְמָה, רָב-כָּעַס; וְיוֹסִיף דַּעַת, יוֹסִיף מַכְאוֹב.

TABLE OF CONTENTS

ABSTRACT

Beta band (13-30 Hz) oscillations in sensorimotor cortex are associated with motor performance, but the nature of this relationship is not clear. Recently, excessive beta activity in cortico-basal ganglia circuits has been recognized as a hallmark of Parkinson's disease. Renewed interest in beta oscillations has since led to the suggestion that they might reflect the preservation of the current output or state of a given brain region. To investigate the potential role of beta activity in the brain, we recorded local field potentials in the frontal cortex and striatum of monkeys as they performed single and sequential arm movement tasks. To facilitate these experiments, we developed novel methods for recording simultaneously from independently moveable electrodes implanted chronically at over 100 sites in cortical and subcortical areas of the monkey brain. We found that, across tasks, beta oscillations occurred in brief, spatially localized bursts that were most prominent following task performance. Across brain regions, post-performance bursts were differentially modulated by the preceding task. In motor cortex they tracked the number of movements just performed. In contrast, striatal and prefrontal burst rates were proportional to the number of visual cues, or to a combination of the cues and movements, respectively, and were higher following correct, rewarded, trials than unrewarded errors. Pairs of striatal-prefrontal sites exhibited increased cross-covariance and coherence during post-trial beta bursts, suggesting that these bursts might be involved in communication or coordination across brain regions. Based on our results, we propose that beta oscillations may represent post-performance reinforcement of the network dynamics that led to the desired behavioral outcome obtained immediately prior.

CHAPTER I

Background and Significance

Neural activity is characterized by oscillations at multiple time-scales. A growing body of evidence implicates oscillatory neural activity in an array of behavioral and cognitive functions, as well as in clinical manifestations of neurological disorders. Recent work has focused on the roles of hippocampal theta (4-7 Hz) and cortical gamma (> 35 Hz) activity in navigation and attention, respectively. The function of activity in the beta band, in between these well-characterized frequency ranges, remains less clear (Engel and Fries, 2010). Beta activity has been studied primarily in motor areas of the cortex and basal ganglia (subthalamic nucleus, STN, and globus pallidus, GP), and only recently in the striatum (Courtemanche et al, 2003). The mechanistic origins of beta oscillations in frontal cortex and basal ganglia are unknown, though they are thought to arise from the interplay of excitatory and inhibitory feedback (Tsai et al., 2008). In the basal ganglia, computational work has identified the GPe-STN network as a likely candidate generator of beta oscillations, which can arise from the inhibition of STN by GPe, coupled with the excitation of GPe by the STN (Nevado Holgado et al., 2010). *In vitro* slice work suggests that beta oscillations in sensorimotor cortex may reflect gap-junction-dependent firing of pyramidal cell layer neurons (Roopun et al., 2006), a view that is supported by the coherence observed between LFPs and hand muscle activity in monkeys during maintenance of a precision grip (Baker et al., 1997).

Two main beta-range phenomena have been described in the literature. First, studies have shown that LFPs in cortical sensorimotor areas of humans (Neuper et al., 2006) and monkeys (Baker et al., 1997; Sanes & Donoghue, 1993; Rubino et al., 2006) follow a pattern of peri-movement ERD and ERS, as described in Specific Aims. Following an instructional cue, there is a consistent decrease in beta power that reaches a

minimum (ERD) around the movement and then rebounds (ERS) before returning to a "resting" baseline (**Fig. 1**). Second, recent studies of the basal ganglia in human Parkinson's disease (PD) patients and animal models have reported increased synchrony in the beta range (Hammond et al., 2007). While the clinical consequences of high beta synchrony in the cortex and basal ganglia are not clear, evidence has been mounting that it can be reduced by the leading treatments for PD, whose pathology involves a loss of the major source of dopanimergic input to the striatum. Remarkably, recent studies have shown that decreases in beta activity in the subthalamic nucleus can correlate with decreases in motor symptoms of PD, specifically bradykinesia and rigidity (Kuhn et al., 2008).

Three main ideas have emerged regarding the functional role of beta activity. First, the classical idea of beta oscillations as the hallmark of an "idling" motor cortex arose from the observation of ongoing beta oscillations during rest, which are suppressed around voluntary movement (Jasper and Penfield, 1949; Pfurtscheller et al., 1996). Second, beta oscillations have been interpreted as being directly "anti-kinetic" (Brown and Williams, 2005), in view of the ERD phenomenon, as well as the elevated levels of beta synchrony in PD and the evidence of a specific link between high cortical beta power and bradykinesia (Pogosyan et al., 2009). Recently, a third hypothesis posited a role for beta oscillations in promoting the status quo (Gilbertson et al, 2005; Engel & Fries, 2010) when the brain does not expect a forthcoming change in sensorimotor set.

These ideas are largely based on recordings of beta from motor areas of the cortex during the performance of simple motor tasks. It is difficult to reconcile these ideas with the few observations of beta phenomena that have been reported outside the traditional

motor areas during performance of more sophisticated behaviors, including the findings of increased beta-range coherence between cortical areas in free vs. instructed search (Pesaran et al., 2008) and of beta as a clocking mechanism in prefrontal cortex (Buschman & Miller, 2009). It is likely that the differences in functional roles ascribed to beta oscillations are due at least in part to differences in brain areas or behavioral tasks. In this thesis we will search for a single interpretation of beta activity that accounts for the patterns of modulation observed across motor and non-motor brain regions in a set of behavioral tasks involving single and sequential arm movements. We will use our results to discover whether the function of beta activity differs across brain regions.

To date, the patterns of beta activity in many of these brain regions have not been reported. This lack of data on beta activity in non-motor brain regions is striking given that several of the published reports on beta activity during movement behavior include speculation about the effects of attention or planning on the observed activity (e.g., Sanes & Donoghue, 1993; Donoghue et al., 1998). This is supported by studies of human cortical sensory areas that reported influences of attention on the power in the alpha (8-14 Hz, Kelly et al., 2006), and to a lesser extent, the beta range (Jones et al., in press). In particular, power in these areas appears to be inversely related to the degree of spatial or somatic attention. In primary motor cortex (M1), the ERD has been reported to follow a brief peri-cue increase in beta power (Rubino et al., 2006), thought to be related to planning or preparation. Recently, 10-45 Hz oscillations in monkey M1 have been shown to phase-lock to the onset of a visual target for arm movement (Reimer & Hatsopoulos, 2010). The degree to which the spiking of individual neurons became phase-locked to the "event-locked" oscillations was correlated with the amount of stimulus-related

information that could be extracted from the spikes, suggesting a role for beta oscillations in the transfer of sensory information to motor cortex.

Taken together, these observations emphasize the need to study beta activity in non-motor areas during performance of movement tasks specifically designed to isolate cognitive functions from motor execution. The purpose of this thesis is to begin to address this need. Some of the main questions we will attempt to answer are: What is the time-course of beta activity across multiple brain regions involved in voluntary motor behavior? To what extent is beta activity spatially localized across and within brain regions? Are there temporal relationships between beta activity patterns across distributed sites? These questions can be addressed experimentally by using behavioral tasks where movement execution can be separated from cognitive aspects of behavior, such as planning and engagement (concentration), and by recording from brain regions that are not predominantly motor-related, such as the dorsolateral prefrontal cortex (dlPFC) and caudate nucleus (CN). In order to discover the functional roles of beta oscillations in frontal cortex and striatum, we recorded LFP activity simultaneously from multiple sites across these structures as macaques performed a set of joystick tasks requiring them to execute single or sequential movements or to withhold movement in response to visual cues. We will focus on characterizing beta activity in primary motor and dorsal premotor cortex (M1PMC), dlPFC and striatum (CN and putamen), a major input stage of the basal ganglia. These structures are thought to be involved in higher-level cognitive processing and specifically in sequencing. Additionally, the involvement of the basal ganglia in PD, along with the observation of excessive beta activity in PD, makes the striatum and the frontal areas anatomically connected to it natural targets for studying beta in the normal

brain. We expect that by characterizing beta activity in these structures in relation to a variety of sequential and single movement tasks, we will be able to assess the functional role of beta activity in frontal cortex and striatum.

REFERENCES

Baker, S.N., Olivier E. & Lemon R.N. Coherent oscillations in monkey motor cortex and hand muscle EMG show task-dependent modulation. *J Physiol* **501**, 225-41 (1997).

Brown, P. & Williams, D. Basal ganglia local field potential activity: Character and functional significane in the human. *Clin Neurophysiol* **116**, 2510-2519 (2005).

Buschman, T.J. & Miller, E.K. Serial, covert shifts of attention during visual search are reflected by the frontal eye fields and correlated with population oscillations. *Neuron* **63**, 386-396 (2009).

Courtemanche, R., Fujii, N. & Graybiel, A.M. Synchronous, focally modulated beta-band oscillations characterize local field potential activity in the striatum of awake behaving monkeys. *J Neurosci* **23**, 11741-11752 (2003).

Donoghue, J.P., et al. Neural discharge and local field potential oscillations in primate motor cortex during voluntary movements. *J Neurophysiol* **79**, 159-173 (1998).

Gilbertson, T., et al. Existing motor state is favored at the expense of new movement during 13-35 Hz oscillatory synchrony in the human corticospinal system. *J Neurosci* **25**, 7771-7779 (2005).

Hammond, C., Bergman H. & Brown, P. Pathological synchronization in Parkinson's disease: networks, models and treatments. *Trends Neurosci* **30**, 357-364 (2007).

Huang, N.E., et al. The empirical mode decomposition and the Hilbert spectrum for nonlinear and non-stationary time series analysis. *Proc R Soc Lond A* **454**, 903-995 (1998).

Huang, N.E., et al. A confidence limit for the empirical mode decomposition and Hilbert spectral analysis. *Proc R Soc Lond A* **459**, 2317-2345 (2003).

Jasper, H.H. & Penfield, W. Electrocorticograms in man: effect of the voluntary movement upon the electrical activity of the precentral gyrus. *Arch Psychiat Z Neurol* **183**, 163-174 (1949).

Jones S.R., et al. Cued spatial attention drives functionally-relevant modulation of the mu rhythm in primary somatosensory cortex. *J Neurosci* (in press).

Kelly, S.P., et al. Increases in alpha oscillatory power reflect an active retinotopic mechanism for distracter suppression during sustained visuospatial attention. *J Neurophysiol* **95**, 3844-3851 (2006).

Kopell, N., et al. Gamma rhythms and beta rhythms have different synchronization properties. *PNAS* **97**, 1867-1872 (2000).

Kuhn, A.A., et al. High-frequency stimulation of the subthalamic nucleus suppresses oscillatory beta activity in patients with Parkinson's disease in parallel with improvement in motor performance. *J Neurosci* **24**, 6165-6173 (2008).

Neuper, C., Wortz, M. & Pfurtscheller, G. ERD/ERS patterns reflecting sensorimotor activation and deactivation. *Prog Brain Res* **159**, 211-222 (2006).

Nevado Holgado, A.J., Terry, J.R. & Bogacz, R. Conditions for the generation of beta oscillations in the subthalamic nucleus-globus pallidus network. *J Neurosci* **30**, 12340-12352 (2010).

Pesaran, B., Nelson, M.J. & Andersen, R.A. Free choice activates a decision circuit between frontal and parietal cortex. *Nature* **453**, 406-410 (2008).

Pogosyan, A., et al. Boosting cortical activity at beta-band frequencies slows movement in humans. *Curr Biol* **19**, 1637-1641 (2009).
Pfurtscheller, G., Stancak, Jr., A. & Neuper C. Post-movement beta synchronization. A correlate of an idling motor area? *Electroencephal Clin Neurophysiol* **98**, 281-293 (1996).
Reimer, J. & Hatsopoulos, N.G. Periodicity and evoked responses in motor cortex. *J Neurosci* **30**, 11506-11515 (2010).
Roopun, A.K., et al. A beta2-frequency (20-30 Hz) oscillations in nonsynaptic networks of somatosensory cortex. *PNAS* **103**, 15646-15650 (2006).
Rubino, D., Robbins, K.A. & Hatsopoulos, N.G. Propagating waves mediate information transfer in the motor cortex. *Nat Neurosci* **9**, 1549-1557 (2006).
Sanes, J.N. & Donoghue, J.P. Oscillations in local field potentials of the primate motor cortex during voluntary movement. *PNAS* **90**, 4470-4474 (1993).
Tsai, T.Y-C., et al. Robust, tunable biological oscillations from interlinked positive and negative feedback loops. *Science* **321**, 126 –129 (2008).

CHAPTER II

A system for recording neural activity chronically and simultaneously from multiple cortical and subcortical regions in non-human primates

Joseph Feingold[1,2]*, Theresa M. Desrochers[2,3]*, Naotaka Fujii[4]*, Ray Harlan[5], Patrick L. Tierney[2,3], Hideki Shimazu[2,3], Ken-ichi Amemori[2,3] and Ann M. Graybiel[2,3]

* These authors contributed equally to this work

[1]HST, MIT, Cambridge, MA, USA

[2]MIBR, MIT, Cambridge, MA, USA

[3]BCS, MIT, Cambridge, MA, USA

[4]BSI, RIKEN, Saitama, Japan

[5]Specialty Machining, Inc., Wayland, MA USA

ABSTRACT

A major goal of neuroscience is to understand the functions of networks of neurons in cognition and behavior. Recent work has focused on implanting fixed arrays of ~100 electrodes or smaller numbers of individually adjustable electrodes, designed to target a few cortical areas. We have developed a recording system that allows the independent movement of hundreds of electrodes chronically implanted in several cortical and subcortical structures. We have tested this system in macaque monkeys, recording simultaneously from up to 127 electrodes in 14 brain areas for up to one year at a time. A key advantage of the system is that it can be used to sample different combinations of sites over prolonged periods, generating multiple snapshots of network activity from a single implant. Used in conjunction with microstimulation and injection methods, this versatile system represents a powerful tool for studying neural network activity in the primate brain.

INTRODUCTION

Microelectrode-based recording techniques provide the most direct measure of electrical activity in the brains of behaving animals. Extracellular recordings of neural signals in the awake, behaving monkey, pioneered by Evarts (Evarts 1968), have shaped our understanding of how the primate brain operates as animals perceive the world, make decisions, and select appropriate actions to reach goals. Despite their remarkable contributions to neuroscience, these classic single-electrode recording methods fall short of the capability of measuring the activity of many neurons simultaneously. Solving this problem is critical, given the widely recognized need to analyze neural computations across distributed networks (Alexander et al. 1986; Cohen and Maunsell 2009; Pesaran et al. 2008), including both cortical and subcortical nodes, the interactions among which are crucial to the function of the entire network (Contreras et al. 1996; Pennartz et al. 2009; Siapas et al. 2005; Sommer and Wurtz 2008) and to the pathophysiology of major neurological diseases (Graybiel and Rauch 2000; Hammond et al. 2007; Rivlin-Etzion et al. 2006).

In order to increase the number of simultaneously recorded sites in the monkey brain, three approaches have been pursued. First, neuronal activity has been recorded simultaneously from multiple brain structures (Hernandez et al. 2008; Pasupathy and Miller 2005) or from multiple sites within a single structure (Baker et al. 1999; Courtemanche et al. 2003; Gray et al. 2007) in acute preparations. Second, chronically implanted arrays of immovable electrodes have increased rates of data acquisition by at least one order of magnitude over acute single electrode techniques (Nicolelis et al. 2003; Nordhausen et al. 1996; Suner et al. 2005; Vetter et al. 2004; Ward et al. 2009). The

pioneering use of these arrays has led to new insights into the correlated activity of multiple neurons (Cohen and Maunsell 2009), as well as to novel therapies centered on brain-machine interfaces for human patients (Carmena et al. 2003; Hochberg et al. 2006; Velliste et al. 2008). Third, small numbers of chronically implanted adjustable-depth electrodes have been used to afford some control over the placement of electrodes post-implantation (Jackson and Fetz 2007; Sun et al. 2006; Swadlow et al. 2005). Other techniques (deCharms et al. 1999; Ecker et al. 2010; Lei et al. 2004), including those adapted from methods used in rodents (Jog et al. 2002; Johnson and Welsh 2003; Yamamoto and Wilson 2008), have begun to be scaled up to record simultaneously from more than one structure in the monkey.

There remains, however, a key need to permit the independent movement of large numbers of electrodes implanted for prolonged periods of time in multiple brain structures. To address this need, we developed a system for recording simultaneously from hundreds of independently movable electrodes implanted in cortical and subcortical sites in the monkey. Using this Chronic Independently Movable Electrode (ChIME) system, we recorded from up to 127 electrodes simultaneously in 14 brain regions with implants lasting up to a year. Like chronically implanted arrays, the ChIME system allows repeated sampling of the same sites from session to session, and like acute methods, it enables the sampling of multiple sites along individual recording tracks, providing an opportunity to improve the unit isolation at each site by adjusting the depth of the electrode. The implant procedure is reversible, and individual monkeys can receive multiple implants in succession, with different configurations of microdrives, targeting the same or different brain regions. The ChIME system is straightforward to use and

highly flexible – the number and locations of the microdrives can be completely reconfigured implant-to-implant, and the microdrives can be used with many different types of electrodes and in combination with electrical stimulation, pharmacological injection and optogenetic techniques. These are essential tools for determining the function of interconnected networks in the brain. The ChIME system thus represents a novel synthesis of numerous critical capabilities into a single, integrated platform suitable for studying the electrophysiology of the non-human primate brain – the definitive animal model for the human brain.

MATERIALS and METHODS

Surgical procedures. Procedures were performed under sterile conditions on anesthetized monkeys placed in a standard stereotaxic apparatus, in accordance with National Institutes of Health guidelines and as approved by the Massachusetts Institute of Technology's Committee on Animal Care. Prior to the chamber implant procedure, in a separate procedure, a mold of the skull was made (VP Mix, Henry Schein) and subsequently used to create a plastic chamber (Delrin, DuPont, DE; Specialty Machining, Wayland, MA). The curved bottom surface of the chamber was machined to fit the contours of the skull precisely. Based on pre-operative MRI of the monkey (T1 and T2 weighted structural images, 1.5-3 Tesla, Siemens, Germany) and in accordance with Rhesus monkey atlases, the chamber was positioned under stereotaxic guidance to facilitate recordings from target brain areas. The chamber could be placed to allow recording either from a single hemisphere or from both hemispheres. During the initial procedure, a portion (10 mm x 20 mm) of the skull was removed over the intended recording area in each hemisphere. The chamber was then secured to the skull with radiopaque bone cement (Palacos, Zimmer, OH), anchored by ceramic screws (Thomas Recording, Germany). Divots around the outside of the lower portion of the chamber facilitated the adhesion of the bone cement. The chamber was designed so that the bottom of the removable grid into which the microdrives can be inserted would be ~10 mm above the highest point on the skull, leaving room for fluid to escape through the side ports, rather than rise above the grid. The placement of the chamber was confirmed post-operatively with structural MRI.

At least one month after the chamber implant, the remaining bone covered by the chamber was removed in one or more procedures. Ultimately, sufficient bone was removed to allow access to the entire volume of brain beneath the chamber, resulting in a single opening in the skull of up to 1600 mm^2. Following recovery, additional physiological mapping was performed to reconfirm the 3D coordinates of the brain in relation to the grid. Additional procedures were performed periodically in order to remove growing bone and to thin the dura mater and overlying granulation tissue.

Electrophysiological mapping. Initially, under the guidance of structural MRIs, the cortex and striatum of each monkey was mapped to determine the locations relative to the grid of known brain landmarks. In each mapping session, a 7 mm thick rectangular plastic grid (area: 30 x 30 mm^2, 30 x 40 mm^2, 30 x 50 mm^2 or 40 x 40 mm^2, Specialty Machining, Wayland, MA, Fig. 1*A*) was inserted into the recording chamber and secured in place with a screw in each corner. Depending on the size of the grid, its holes (0.025 in diam., spaced 1 mm center-to-center) could provide access to the brain across an area of up to 1600 mm^2. The holes in some grids were offset such that a 90° rotation would provide access to tracks that are shifted by 0.5 mm from those accessible in the original orientation. This design enabled sampling from non-overlapping recording tracks when accessing the underlying brain through the same grid holes in successive chronic implants.

In each mapping session, up to 12 epoxy-insulated tungsten microelectrodes (Frederick Haer, Inc., ME, 1-2 MOhm at 1 kHz, 110 to 130 mm long, 125 μm shank, ~3 μm diam. tip) glued to screw microdrives (Fig. 1*A*) were acutely implanted in the brain,

using sharp stainless steel guide-tubes to penetrate the dura mater while protecting the tips of the electrodes. Neuronal responses were characterized by standard somatosensory, visual and auditory tests and by manipulation of the limbs and electrical microstimulation (Master-8, A.M.P.I., Israel, and Bak Electronics, MD, trains of 24-64 250 μs wide biphasic pulses, 333 Hz, 10-150 μA). Several sessions were performed to map the somatotopic organization of the motor and oculomotor cortical areas, including M1 (Strick and Preston 1982), FEF (Funahashi et al. 1989; Sommer and Wurtz 2000), SMA and pSMA (Luppino et al. 1991; Matsuzaka et al. 1992; Mitz and Wise 1987), and to confirm the depths of the CN, Put and other subcortical targets, as needed. The dlPFC was defined as the area rostral to the FEF, surrounding the principal sulcus and corresponding to Brodmann Area 9/46.

Chronic implant preparation. Depending on the experiment and based on the MRIs and the results of electrophysiological mapping, the desired number and locations of electrodes were selected. The electrodes were loaded onto custom-made screw-based microdrives (Specialty Machining, Wayland, MA). Each microdrive consisted of 1-3 groups of three adjacent screws each (length, 0.825 in; 160 threads per inch, so that six 360° turns = 0.9525 mm of vertical travel distance), spaced 1 mm apart, and supported by a plastic frame. A pair of stainless steel pins on the bottom of the microdrive frame fit into grid holes and was used to secure the microdrive to the grid inside the chamber rigidly. The microdrive was designed so that the heads of the screws were flush with the top of the microdrive, and could be turned with a flat-head screwdriver (Fig. 1*B-E*). Each screw was threaded through a 5 mm-long plastic sled with a slot to which one or more

electrodes could be glued. The screws rested on the bottom of the microdrive frame, so that turning a screw would cause the attached sled to move along the screw's shaft. The microdrive's plastic frame provided friction to prevent the sleds on the outer screws of each group of three from twisting around the screw threads. The sleds on neighboring screws provided additional stabilizing friction, so long as the center-points of the sleds were less than a sled's length apart in height. The sleds guided the electrodes through the grid holes in a row immediately adjacent to the grid holes occupied by the microdrive itself.

Prior to an implant procedure, the grid was prepared in the following manner. First, the entire top and under side of the grid was covered in a general purpose silicone sealant to prevent fluid from below the grid from contaminating the space above the grid. After curing, the silicone was cleared with a 23-gauge needle from the grid holes needed for the implant. Bare copper wire for carrying the ground was looped below the grid and the free ends were fed through the cleared grid holes and capped with pins to interface with the connectors. In some implants, the copper wire was soldered to a piece of flattened copper mesh, designed to rest over as large a portion of the granulation tissue as possible (without obstructing the path of the electrodes). The outer guide-tubes (23-gauge, extra thin wall) of a set of two telescoping guide-tubes designed to protect each electrode were then inserted into the holes cleared for electrode tracks. These tubes were short enough so that they would not touch the surface of the granulation tissue above the dura. To carry reference signals, a number of electrodes or 23-gauge stainless steel tubes that could reach the tissue under the grid were inserted through cleared grid holes. The entire grid construct was bathed in 70% ethyl alcohol prior to the implant procedure.

The microdrives and electrodes were prepared in parallel with the grid. First, connector pins were crimped onto the ends of the electrodes (same as mapping electrodes or Parylene-coated tungsten or platinum/iridium (Pt/Ir), 125 μm shank diameter, impedance < 1.5 MΩ, WeSense, Israel) and then glued (2-hour epoxy, extra slow cure). Second, the impedance of each electrode was tested to confirm that it fell within the acceptable range (0.5-1.5 MOhms). Third, each electrode was glued to a slotted sled on one microdrive screw, so that, upon implanting, the recording tip of the electrode would be at the desired depth relative to the grid. After the glue cured, securing the electrodes to the microdrive, a sharp-edged stainless-steel guide-tube (27-gauge, regular wall hypodermic disposable needle or custom cut and beveled tubing) was slipped over the shank of each electrode and left covering the tip to protect it during the implant procedure. The guide-tubes were filled with mineral oil to keep out blood and other fluids. The electrode leads of each loaded microdrive were grouped together by microdrive using labeled, folded paper slips, intended to prevent the leads from tangling during the implant procedure.

Chronic implant procedure. The implant procedure was performed under aseptic conditions, with the monkey under light general anesthesia (ketamine, xylazine and atropine) and the head fixed within a stereotaxic apparatus. After thoroughly cleaning and drying the chamber and the grid, silicone sealant was applied around the outer edge of the grid. The grid was inserted into the chamber and secured to it with four screws and washers in the corners. Then, one by one working from the center of the implant outward, each microdrive was carefully positioned above the target grid holes. The 27-gauge

guide-tubes covering the electrode tips were lowered into the 23-gauge guide-tubes that had already been inserted into the grid. Once all the sharp guide-tubes for a given microdrive were properly situated, they were used to punch small holes through the dura mater, using forceps or fine needle holders. The microdrive was then slowly lowered into position and its bottom pins were fit into the grid holes, so that the bottom of the microdrive frame was flush with the surface of the grid. Openings in the sides of the chamber were used to monitor the tissue underlying the grid and remove any excess fluid during this process.

Upon completion of the implantation of all the electrodes, a bead of silicon sealant was applied along the upper junction of the chamber and grid and the grid anchor screws covered. Any cleared holes in the grid not filled by implant components were also filled in. Then the pins from the ends of the electrode leads, references, and ground wires were plugged into the appropriate spots along the connector strips. Efforts were made to minimize crisscrossing of the leads above the microdrives. Finally, all the wires were carefully bent with forceps in order to accommodate the connectors fastened to the edges of the chamber, and a thick coat of varnish was applied to protect and insulate them (completed implant, Fig. 1*C*). Plastic spacers (Fig. 1*A*,*C*,*D*) were used in between the connectors to adjust their heights as necessary to accommodate the preamplifiers. The location of holes used to screw the connectors to the chamber and the dimensions of the plastic spacers could easily be adjusted to accommodate different sizes or configurations of preamplifiers.

Recording sessions and implant maintenance. During the first few weeks of a chronic implant, electrodes were slowly lowered to their initial recording positions in the brain, the earliest points at which unit activity could be detected in the target structures. Once a sufficiently large fraction of electrodes had reached their targets, recordings commenced in daily sessions. Either at the start of recording sessions or in between them (on non-recording days), a subset of electrodes was advanced carefully in ~20 μm steps to isolate units. Typically, on any given day no more than approximately 1/3 of the total electrodes in the implant were moved, and an effort was made not to move adjacent electrodes in order to promote the stability of recordings.

Large slots in the lower portion of the chamber (Fig. 1*A*) provided access to the underside of the grid for daily cleaning and observation of the surface of the granulation tissue, which had grown to cover the dura mater. This granulation tissue effectively sealed the brain from the underside of the grid and chamber. At the start of each session, the chamber beneath the grid was flushed thoroughly with sterile saline via these side ports. Depending on the monkey and the chronic implant, this was followed by diluted (20:1) Novalsan Solution (chlorhexidine diacetate 2%) or Betadine Solution (povidone-iodine 10%) 2-5 times per week. Possible infections, as indicated by the type and amount of discharge, were treated with dilute antibiotic applied inside the chamber. Systemic administration of antibiotics was rarely used. Topical antibiotic ointment was occasionally applied along the margins of the chamber. With these precautions, the chambers could be maintained for up to five years (Chamber Lifetime, Table 1).

The chamber beneath the grid was filled with saline for the duration of the session. Prior to some sessions, the saline was mixed with viscous methyl cellulose, in

order to reduce noise resulting from the motion of the saline. When necessary, application of petroleum jelly or silicon grease to the electrode leads between the tops of the microdrives and the connectors effectively dampened mechanical vibrations of the electrodes. Additionally, if fluid were suspected of traveling up the guide tubes to the surface of the grid, silicon grease was used to fill the space between the electrodes and guide tubes, sealing the tops of the tubes, while permitting the free movement of the electrodes.

Over the course of the implant, the space above the grid was kept as dry and clean as possible, in order to preserve the quality of recorded signals and the ability to manipulate the depths of electrodes with the microdrives. The grid was sealed with silicone and the side slots in the chamber beneath the grid were left partially open, as needed, to minimize fluid build-up. Further protection from fluid was provided by a raised ridge around the top of the inner surface of the chamber (surrounding the grid) that served as a dam.

In between experimental sessions, the chamber was covered with either a raised cap, while electrodes were implanted in the brain, or a flat cap, otherwise (Fig. 1*A* top). The side panels on the raised cap could be removed to connect pre-amplifiers to the connector strips without having to remove the main portion of the cap. Ventilation slots along the non-removable ends of the raised cap helped to keep the space above the grid dry.

Neuronal signals were amplified and filtered (600-6000 Hz for spikes, and 1-475 Hz for LFPs) by the Cheetah system (Neuralynx Inc., Bozeman, MT). Spike waveforms (32 kHz sampling rate) and LFP signals (2 kHz) were continuously collected during daily

recording sessions. The Cheetah system was configured to accommodate up to 128 single electrodes along with 8 analog input channels (for behavioral data). At the start of each recording session, custom software was used to configure each electrode channel to record either spike or LFP data. Spike and LFP signals could be recorded simultaneously from up to 32 electrodes. Each neural (spike or LFP) data channel was stored to a separate file for offline analysis.

In some implants, the impedance of the electrodes was measured periodically and those with high impedance (> 2 MOhm) were stimulated (Master-8, A.M.P.I., Israel, and Bak Electronics, MD, 100-200 ms trains of biphasic pulses at 1 kHz, < 20 μA). Stimulation was repeated up to five times or until the impedance fell below 2 MOhm. Post-stimulation impedance values were measured and recorded.

Electrical stimulation experiments. The ACC stimulation experiments were conducted with a chronic implant of 48 independently movable electrodes targeting the ACC, CMA, CN and dlPFC. In each trial a single bipolar, biphasic pulse (current amplitude: 200 μA, cathodal-anodal pulse duration: 400 μs) was delivered between two of the Pt/Ir electrodes chronically implanted in the ACC (4 mm apart). The responses of single units in the ACC and CMA were analyzed by binning the spike counts of each unit in a 20 ms window surrounding the stimulus delivery. The analysis was repeated for two bin sizes (0.1 ms and 1 ms). Bins with spike counts beyond the 99% confidence limits were defined as statistically significant. Those units exhibiting significant responses irrespective of bin size were considered to be modulated significantly by the electrical stimulation.

Stimulation experiments in the dlPFC were performed with a chronic implant of 24 independently movable tungsten electrodes (12 each in dlPFC and CN). Four of the dlPFC electrodes (2 each in areas 9L and 46) were used for delivering electrical stimuli. In each of 40 trials, spaced 5 s apart, a single monopolar, biphasic pulse (current amplitude: 20 μA, cathodal-anodal pulse duration: 300 μs) was delivered. LFPs were recorded from eight electrodes in the CN (2 mm apart in a 4x4 configuration). LFPs were low-pass filtered at 20 Hz and stimulation-triggered waveform averages were computed on 400 ms of LFP data centered on the onset of stimulation. Significant modulation of waveform averages was detected by comparing the post-stimulation activity to the 95% confidence limits estimated from the pre-stimulation activity.

Pharmacological microinjection experiments. A microelectrode nested within a steel canula was used to record electrophysiological activity during local drug infusion. The canula was connected via polyethylene tubing to a tabletop pump (Harvard Apparatus, Cambridge, MA). Drugs were delivered at a rate of 100 nL/min for 2 minutes. Periods of significant changes in firing rate were detected using a sliding bin average, as follows. Spike counts were aggregated into 10 s bins and the bin values underwent 3-point smoothing. Baseline activity was defined as the mean bin value over the 5 min immediately preceding drug infusion. The onset of a significant change in firing rate was defined as the 1st of 10 consecutive bins with values at least 2 s.d. from the baseline. Response offset was defined as the 1st of 10 consecutive bins with values within 2 s.d. of the baseline.

Implant removal. At the end of a chronic implant, the electrodes were slowly raised to their initial depths, over a few sessions. With the alert monkey head-fixed, the implant was then removed in a single procedure. First, the electrode leads above the microdrives and reference and ground wires were cut, and the connector strips unscrewed from the chamber. Then, each microdrive was removed by first ensuring the electrodes are retracted as far as possible, if possible using forceps to raise guide-tubes and then gently using force perpendicular to the grid to extract the manipulator. Once all the manipulators have been removed in this manner, the silicon sealing the grid was stripped away and the grid itself removed by unscrewing the corner screws. The chamber was then thoroughly rinsed with sterile saline. The monkey was allowed to recover for at least a few weeks before the next implant. The grid, microdrives and most 23-gauge guide-tubes that could be recovered for use in subsequent implants were cleaned with ethanol, bleach and acetone. If needed, prior to the next implant, a small drop of oil was added to each of the plastic sleds that travel along the microdrive screws, in order to ensure free movement of the sled and minimal wear and tear on the plastic.

Histology. After experiments were completed, the monkey was perfused intracardially with fixative (0.9% NaCl followed by 4% paraformaldehyde in 0.1 M Na^{2+}/K^{-} PO_4 buffer, pH 7.4). Whenever possible, this was done before removing the final chronic implant. In some cases, electrolytic lesions (10 μA DC for 10 s, < 15 sites) were made to mark locations in the brain relative to the grid. Conventional Nissl staining (60 μm thick slices) was performed to visualize electrode tracks. The slices were analyzed to reconstruct the location of each electrode in each recording session. Tracks from earlier

chronic implants were reconstructed on the assumption that the distance from the grid to the surface of the brain was constant across implants. In some monkeys, anatomical tracing software and 3D reconstruction (Neurolucida, MicroBrightField, Inc., Williston, VT) was used.

RESULTS

Reconfigurable chronic electrode implant system

We designed and implemented the ChIME system to obtain simultaneous recordings of neural activity from multiple, individually movable microelectrodes chronically implanted in cortical and subcortical structures of the primate brain. The key components of the ChIME system are compact screw-based microdrives that can be placed in nearly any configuration on a grid (Fig. 1). Improving upon the concept of the widely used (Pasupathy and Miller) method of Wurtz and colleagues (Nichols et al. 1998) for acute, single-electrode recordings, the ChiME microdrives employ a novel mechanism whereby each recording track is targeted by a single screw occupying a single grid hole, thus maximizing the density of independently movable electrodes. The grid can be inserted into a plastic chamber fixed to the skull, in order to deliver electrodes to the underlying brain. Structural magnetic resonance images (MRIs) are used (Fig. 2*A*) to confirm the location of the grid holes relative to the target regions in the brain. We describe here the use of the system based on results from 16 implants of electrodes placed in cortical and subcortical sites in seven monkeys (Table 1). Preliminary experimental results based on the use of pilot versions of the ChIME system have been published elsewhere (Fujii and Graybiel 2005; Fujii et al. 2007).

Microdrives loaded with 3, 6 or 9 individually movable electrodes were placed on grid within the chamber, and the electrodes were lowered into the brain in a single implant procedure (see Methods). Subsequently, across multiple daily sessions, the electrodes were advanced to their intended target sites. The depth of each electrode was controlled by turning the microdrive screw (158.75 μm/turn) to which it was attached.

Implants were left in place for periods of weeks to months, during which the depths of individual electrodes were continually adjusted (maximum travel distance: 13 mm from initial implant depth). Following completion of the recordings, histological analysis was performed to reconstruct the locations of the electrodes (Fig. 2*B-D*).

Simultaneously recorded neural activity from multiple cortical and subcortical sites

To test the ChIME system, we have used implants ranging in size from 27 to 127 electrodes and lasting from 22 to 365 days. In each implant, single-unit spike activity and local field potentials (LFPs) were recorded simultaneously from electrodes implanted in 6-14 brain structures bilaterally, including medial and dorsolateral prefrontal cortex (mPFC and dlPFC), frontal eye fields (FEF), supplementary eye fields (SEF), primary motor cortex (M1), premotor cortex (PM), supplementary and pre-supplementary motor areas (SMA and pSMA), anterior cingulate cortex (ACC), cingulate motor area (CMA), orbitofrontal cortex, parietal cortex, caudate nucleus (CN), putamen (Put), globus pallidus, thalamus and amygdala. Recording sessions occurred on up to 59% of the days an implant was in place. In a single session, up to 57 electrodes recorded unit activity simultaneously along with 84 LFP signals. Under the constraints of the data acquisition system that we used, when fewer units were recorded, up to 127 LFPs were recorded simultaneously.

We used the ChIME system to record neural signals simultaneously from several neocortical and subcortical regions participating in widely distributed brain networks. The left half of Fig. 3 gives examples of LFPs recorded simultaneously from the left hemisphere of a bilateral implant in monkey H, showing different activity patterns across

seven regions, during performance of a joystick movement task. The right half of Fig. 3 shows examples of unit activity recorded simultaneously from the right hemisphere of a separate implant in monkey G, during performance of an oculomotor scan task. For each implant, all of the recording sites were accessed through a single craniotomy and grid.

Session-to-session adjustment of individual electrodes' depths

We have found that electrode depths can be adjusted either immediately prior to a recording session or on a previous day. Manipulating the depths of individual electrodes at different times enabled us to monitor activity from different combinations of sites within multiple regions across the recording sessions performed during a single implant (Fig. 4*A*). The vertical travel of the microdrives (up to 13 mm) enabled individual electrodes to progress through multiple brain structures over the course of a single chronic implant (Fig. 4*B*). Within a given brain structure, it was possible to record from sites at which neurons exhibited different activity profiles along a single track (Fig. 4*C*).

We defined the yield in each recording session as the fraction of electrodes that recorded unit activity. The average yield over all sessions was 31% (Mean Yield, Table 1), but the yield varied from implant to implant, ranging from 18% to 65%. The yield averaged across all implants decreased over months (Fig. 5), though the time-course of the yield differed across implants (Fig. 6). Implants with fewer electrodes and of shorter durations were associated with higher yields (Fig. 6, right vs. left columns; note difference in vertical scale). In most implants the yield converged within a few weeks to the overall mean value (31%).

To investigate the time-course of the yield in individual implants, in each recording session of two monkeys (H and J, 5 implants total), we classified the electrodes that recorded unit activity into two groups: electrodes that had recorded units in the preceding session and electrodes that had not (Fig. 7). These two groups both contributed persistently to the yield over the course of each implant. Of the electrodes that recorded at least one unit in a given session, 35% ± 18% (mean ± s.d. unless otherwise noted) recorded new unit activity, that is, they had not recorded any units in the previous session (means for each implant in Monkey H: 43% ± 16%, 35% ± 21% and 44% ± 12%; in Monkey J: 25% ± 13% and 32% ± 20%). The emergence of new activity on many electrodes represents a key advantage of the ChIME system over fixed multi-electrode arrays, and new unit activity can continue to arise for several months after the start of an implant.

To assess the effect of manipulating the depths of the implanted electrodes on the yield, we present an analysis of data from monkey H, because session yields did not differ significantly across all three implants in this monkey (chi-square test, $P > 0.5$). Of the electrodes that recorded new unit activity in a given session, on average 37% ± 32% had been moved since the preceding session (Fig. 7*A-C*). As this percentage varied with the rate at which electrodes were moved, it does not imply a causal relationship between moving electrodes and recording new unit activity. Focusing on the electrodes that had not recorded units in a given session, we asked whether moving them increased the likelihood of recording new units in the following session. In each of the three implants, we found that it did. Electrodes that had been moved were significantly more likely to record new units in the following session than electrodes that had not been moved (chi-

square test, $P < 10^{-15}$). This comparison likely underestimates the effect of moving electrodes on the yield, as we examined the probability of obtaining unit activity only in the recording session immediately following a session in which an electrode was moved, and we did not take into account the cumulative effects of moving electrodes multiple times before new units were recorded.

Session-to-session stability of neural activity

We tested the ability of the ChIME system to record stable neural activity during consecutive sessions from multiple electrodes that were not moved in the interim (Fig. 8). We analyzed the durations of such stretches of stable activity in six implants across three monkeys. On average, an electrode recorded unit activity in 2.1 ± 2.8 consecutive sessions (3.9 ± 8.5 days) without being moved. Stationary electrodes that recorded unit activity in at least two consecutive sessions recorded unit activity in a total of 4.2 ± 4.1 consecutive sessions (9.7 ± 12.8 days), on average. Such activity was not only stable, but typically exhibited striking similarities in wave-shape, inter-spike interval distribution and responses to task events across sessions (Fig. 8*A*, Days 106-115). LFPs recorded from stationary electrodes also showed extraordinary stability over periods of several weeks to months (Fig. 8*B*). When the electrodes were moved, the recorded signals changed (Fig. 4*B*,*C*; Fig. 8*A* first and last day; Fig. 8*B*, last day), suggesting that the preceding recordings were likely obtained from small volumes of brain with similar functional properties.

Microstimulation and injection using the ChIME system

We have exploited the versatility of the ChIME system to incorporate electrical stimulation and pharmacological injection methods with chronic recordings of neural activity. In a subset of experiments, we tested for within-area modulation of spike activity using single-pulse electrical stimuli in the ACC. We found fixed, short-latency responses from multiple simultaneously recorded units in the ACC, indicating synaptic connectivity between sites targeted by the chronically implanted electrodes (Fig. 9). The stimulation-evoked responses were sufficiently localized, so that units recorded in the CMA did not respond to the ACC stimulation. Moreover, on electrodes that recorded multiple units in the ACC, not all single units exhibited a significant response. In separate experiments, we used electrical stimulation to detect functional connectivity between brain areas. By stimulating at four sites in the dlPFC, we found differential modulation of the LFP activity recorded simultaneously at multiple sites in the CN (Fig. 10*A*).

We have also begun to develop injection methods for use with the ChIME system. In pilot experiments, we recorded units in dlPFC and CN simultaneously and examined their responses to injections made in the CN. In the example shown in Fig. 10*B*, all four of the striatal units exhibited changes in firing rate, whereas none of the eight prefrontal units showed changes in firing rate for up to 10 minutes following the injection. This example demonstrates the possibility of using the ChIME system to perform pharmacological manipulations of subsets of recording sites in the context of an extended-duration implant. Stimulation and injection techniques can be used to search for and identify desired recording sites, as well as to record the neural and behavioral effects of localized electrical or pharmacological manipulations, making the ChIME system a powerful tool for studying the functions of brain circuits.

DISCUSSION

Large-scale simultaneous recordings from multiple superficial and deep brain structures test the limits of existing methods for extracellular recordings in alert non-human primates. We developed the ChIME system to meet this need. The most important advantage of our system is the opportunity it provides to sample neural activity at multiple depths chronically and flexibly. The ability to move individual electrodes can dramatically improve the yield of single units, as demonstrated by the comparison of the unit activity between electrodes that had or had not been moved across pairs of successive sessions. The single-unit yields in the initial recording sessions of each implant were similar to those reported for experiments using fixed-electrode arrays, chronically implanted in multiple cortical areas (Chhatbar et al. 2010; Nicolelis et al.). However, the ability to move electrodes at will over the lifetime of the implant led to sustainably high yields over the long-term, in marked contrast to the typical time-dependent deterioration of yields seen with fixed-electrode arrays. In addition to its critical effect on the yield, the independent manipulation of electrodes enabled recordings from different combinations of depths across the recording tracks of a single implant (Fig. 4). This cannot be done using silicon probes with multiple contacts, the distances between which are fixed (Kipke et al. 2003). Furthermore, fixed arrays have not been used to study subcortical structures of the primate brain because of the substantial damage to the overlying cortex and white matter, as has been observed in the brains of non-primates (McCreery et al. 2006). Finally, whereas there is little control over the types of cells recorded with fixed arrays, by adjusting the depths of electrodes independently

with the ChIME system, cells that are anatomically connected (as confirmed by microstimulation) or that belong to specific classes (based on physiological characteristics and responses) can be targeted and studied selectively. Taken together, the numerous advantages of the movable electrodes implanted with the ChIME system thus provide a unique opportunity to collect neural data for analyzing circuits spanning cortical and deep structures.

The ChIME system is the first to enable simultaneous recordings from chronically implanted electrodes in cortical and subcortical sites in the non-human primate brain, controlled by as many as hundreds of independently movable drives. Other recording methods share some, but not all, of the features of the ChIME system. Jackson and Fetz (Nichols et al. 1998), and separately Wilson and colleagues (Sun et al. 2006), used chronically implanted, independently movable electrodes in the non-human primate. However, these methods were designed for use only with a small number of electrodes, and primarily in the freely moving monkey. A method by Merzenich and colleagues (deCharms et al. 1999) used 49 electrodes, but to record from a single cortical area of non-human primates with brains considerably smaller than those of macaques. It is not clear whether or how any of these or similar methods (Galashan et al.) could be used to record simultaneously from multiple structures in the macaque brain, as we have done using the ChIME system. Other chronic recording methods using movable microwires have been developed for non-primate species, including rabbits (Swadlow et al. 2005) and rodents (Jog et al. 2002; Johnson and Welsh 2003; Yamamoto and Wilson 2008). Adapting these methods to record from multiple cortical and deep structures in the macaque brain would require reducing the physical footprint of the microdrives

substantially, as well as overcoming the challenge of traversing sulci with microwires, as opposed to the sharp microelectrodes used with the ChIME system.

Others have recorded neuronal activity in the monkey brain simultaneously from multiple structures (Buschman and Miller 2007; Hernandez et al. ; Pasupathy and Miller 2005) or from multiple sites within a single structure (Baker et al. 1999; Courtemanche et al. 2003; Gray et al. 2007) using acute methods, in which the electrodes were implanted daily. Recordings commenced within a few hours following electrode implantation, and the electrodes were extracted from the brain at the end of each recording session. These acute multi-electrode methods require considerable preparation time prior to each recording session, constraining the duration and frequency of experimental sessions. These methods have additional drawbacks, including the difficulty of maintaining stable signals following the acute implantation of multiple electrodes in a confined region; an increased potential for tissue damage from repeated daily penetrations of the dura and brain; and the inability to track learning-related changes in the activity of a localized neural population over daily recording sessions. Most importantly, the maximum number of independently movable drives that can be implanted acutely is likely to be at least one order of magnitude smaller than what can be achieved with the ChIME system.

In our experiments using the ChIME system, the neural signals on many electrodes were stable across numerous sessions (Fig. 7,8). The durations of periods of stable activity recorded by individual electrodes were likely limited by the fact that most of the electrodes in an implant were moved periodically, in order to sample new sites along each track. Moving electrodes could have reduced the stability of signals recorded on stationary neighboring electrodes. We suspect that the long-term stability of signals

recorded with the ChIME system is due to the combination of continued growth of granulation tissue overlying the exposed dura mater within the chamber and to the multiple guide-tubes stabilizing the dural surface. It is possible for the dura mater and overlying calvarium to re-grow over the course of several weeks, providing even further stabilization of the electrodes. Indeed, we found evidence for dural adhesions to the guide-tubes in at least one monkey that was perfused with the implanted electrodes left in place (see Methods).

As signal quality was often maintained day-to-day, minimal pre-recording preparation time was required, with the bulk of it spent adjusting electrode depths in order to improve single-unit isolation. On any given day, we only adjusted the depths of a fraction of the electrodes. With implants of greater numbers of electrodes, we moved electrodes only on non-recording days. This made the system essentially "plug-and-play" on recording days, maximizing the length of recording sessions.

The number of electrodes used in our experiments to date has been limited only by the capacity of available data acquisition systems. We have demonstrated the capabilities of the ChIME system using commercially available, epoxy-coated tungsten or parylene-coated platinum/iridium microelectrodes, but we have successfully tested the use of microwire bundles to increase the density of recording sites by increasing the number of recording channels per track. These could be substituted by tetrodes, stereotrodes, or multi-contact probes, all of which can be attached to a microdrive screw. The number of simultaneously recorded channels could also be increased by adding more microdrives, which can drive ~9 tracks per 30 grid holes, allowing up to ~450 tracks in a single implant (using a 40 mm x 40 mm grid).

The flexibility of the ChIME system permits the incorporation of other methods in conjunction with electrode-based recordings. Electrical stimulation can be used to map the functional connectivity within and across brain areas over the course of a chronic implant (Figs. 9,10*A*). Microinjections can be made through the grid to perform pharmacological manipulations and anatomical labeling (Fig. 10*B*). Fiber optics can be passed through the grid for use with optogenetic methods, which have recently been extended to the monkey brain (Diester et al. 2011; Han et al. 2009). With minor changes (e.g., replacing the microdrive screws with plastic ones), the ChIME system could also be used in paired recording and functional MR-imaging experiments. Using these and other innovative techniques with the ChIME system should make it possible to manipulate and record chemical, electrical and optical signals in nearby tracks simultaneously over long periods of time, giving unprecedented insight into the circuit-level functions of cortical and subcortical networks.

The gradual deterioration of signal quality is a challenge facing all chronic recording methods. The fall-off in yield and accompanying increase in the impedance of many electrodes over the course of an implant has been attributed to the process of gliosis (Stice and Muthuswamy 2009). The ChIME system can be used to reduce the effects of gliosis by moving the electrodes. Nevertheless, in our experience, the signal-to-noise ratio tended to degrade over the duration of the implant along with the proportion of well-isolated single units. Using platinum/iridum electrodes, we have been able to reduce electrode impedances by stimulating frequently to "clean" the electrode tips (Otto et al. 2006). The stimulation paradigm effectively reduced even high impedances (> 2 MOhm)

to pre-implant levels. However, stimulation typically did not lead to new unit activity unless the electrodes were subsequently moved.

A potential drawback of the ChIME system, shared by other implant systems, is that the approach of some of the electrodes is not orthogonal to the cortical surface (Fig. 2d). This can present a challenge for targeting some cortical areas. When necessary, we have addressed this issue by implanting some chambers above a single hemisphere, targeting structures along up to 50 mm of the anterior-posterior axis. This orients most of the grid in parallel to the underlying cortical surface. We have also used smaller chambers (e.g., 30 mm x 30 mm), placed at an angle and offset from the midline.

The ChIME system successfully resolves two major problems associated with current recording techniques: a low rate of data acquisition and the inability to measure the activity of many neurons simultaneously across superficial and deep brain structures. The main advantages of our system include: the ability to sample from a variety of cortical and subcortical locations simultaneously; the possibility of changing the recording locations over days; the increased yield resulting from moving electrodes; the ability to sample activity from small volumes of brain with excellent stability over weeks; minimal daily preparation and maintenance; the ability to re-implant monkeys in the same or different brain regions; and the possibility of interfacing with a variety of electrodes and experimental techniques. These key features combine to make a powerful, simple to use, chronic recording system that we anticipate will contribute to an understanding of the function of multiple interacting circuits widely distributed across the brain.

ACKNOWLEDGEMENTS

We thank P. Blazquez, H.F. Hall, M. Cantor, N. Hasegawa, B. DePasquale, A. Quach, P. Harlan, R. Marini, C. Keller-McGandy, M. Histed, Y. Kubota, B. Baker, G. Fakterman, E. Romano, A. McWhinnie and M.C. Brown for their help.

GRANTS

This work was supported by the National Institutes of Health Javits Merit Grant NS025529, National Eye Institute Grant EY012848, Office of Naval Research Grant N000140710903, DARPA Grant NBCHC070105 and the Stanley H. and Sheila G. Sydney Fund (AMG), MIT Zakhartchenko Fellowship (JF) and NDSEG Fellowship (TMD).

REFERENCES

Alexander GE, DeLong MR, and Strick PL. Parallel organization of functionally segregated circuits linking basal ganglia and cortex. *Annu Rev Neurosci* 9: 357-381, 1986.

Baker SN, Philbin N, Spinks R, Pinches EM, Wolpert DM, MacManus DG, Pauluis Q, and Lemon RN. Multiple single unit recording in the cortex of monkeys using independently moveable microelectrodes. *J Neurosci Methods* 94: 5-17, 1999.

Buschman TJ, and Miller EK. Top-down versus bottom-up control of attention in the prefrontal and posterior parietal cortices. *Science* 315: 1860-1862, 2007.

Carmena JM, Lebedev MA, Crist RE, O'Doherty JE, Santucci DM, Dimitrov DF, Patil PG, Henriquez CS, and Nicolelis MA. Learning to control a brain-machine interface for reaching and grasping by primates. *PLoS Biol* 1: E42, 2003.

Chhatbar PY, von Kraus LM, Semework M, and Francis JT. A bio-friendly and economical technique for chronic implantation of multiple microelectrode arrays. *J Neurosci Methods* 188: 187-194, 2010.

Cohen MR, and Maunsell JH. Attention improves performance primarily by reducing interneuronal correlations. *Nat Neurosci* 12: 1594-1600, 2009.

Contreras D, Destexhe A, Sejnowski TJ, and Steriade M. Control of spatiotemporal coherence of a thalamic oscillation by corticothalamic feedback. *Science* 274: 771-774, 1996.

Courtemanche R, Fujii N, and Graybiel AM. Synchronous, focally modulated beta-band oscillations characterize local field potential activity in the striatum of awake behaving monkeys. *J Neurosci* 23: 11741-11752, 2003.

deCharms RC, Blake DT, and Merzenich MM. A multielectrode implant device for the cerebral cortex. *J Neurosci Methods* 93: 27-35, 1999.

Diester I, Kaufman MT, Mogri M, Pashaie R, Goo W, Yizhar O, Ramakrishnan C, Deisseroth K, and Shenoy KV. An optogenetic toolbox designed for primates. *Nat Neurosci* 2011.

Ecker AS, Berens P, Keliris GA, Bethge M, Logothetis NK, and Tolias AS. Decorrelated neuronal firing in cortical microcircuits. *Science* 327: 584-587, 2010.

Evarts EV. Relation of pyramidal tract activity to force exerted during voluntary movement. *J Neurophysiol* 31: 14-27, 1968.

Fujii N, and Graybiel AM. Time-varying covariance of neural activities recorded in striatum and frontal cortex as monkeys perform sequential-saccade tasks. *Proc Natl Acad Sci U S A* 102: 9032-9037, 2005.

Fujii N, Hihara S, and Iriki A. Dynamic social adaptation of motion-related neurons in primate parietal cortex. *PLoS ONE* 2: e397, 2007.

Funahashi S, Bruce CJ, and Goldman-Rakic PS. Mnemonic coding of visual space in the monkey's dorsolateral prefrontal cortex. *J Neurophysiol* 61: 331-349, 1989.

Galashan FO, Rempel HC, Meyer A, Gruber-Dujardin E, Kreiter AK, and Wegener D. A new type of recording chamber with an easy-to-exchange microdrive array for chronic recordings in macaque monkeys. *J Neurophysiol* 2011.

Gray CM, Goodell B, and Lear A. Multichannel micromanipulator and chamber system for recording multineuronal activity in alert, non-human primates. *J Neurophysiol* 98: 527-536, 2007.
Graybiel AM, and Rauch SL. Toward a neurobiology of obsessive-compulsive disorder. *Neuron* 28: 343-347, 2000.
Hammond C, Bergman H, and Brown P. Pathological synchronization in Parkinson's disease: networks, models and treatments. *Trends Neurosci* 30: 357-364, 2007.
Han X, Qian X, Bernstein JG, Zhou HH, Franzesi GT, Stern P, Bronson RT, Graybiel AM, Desimone R, and Boyden ES. Millisecond-timescale optical control of neural dynamics in the nonhuman primate brain. *Neuron* 62: 191-198, 2009.
Hernandez A, Nacher V, Luna R, Alvarez M, Zainos A, Cordero S, Camarillo L, Vazquez Y, Lemus L, and Romo R. Procedure for recording the simultaneous activity of single neurons distributed across cortical areas during sensory discrimination. *Proc Natl Acad Sci U S A* 105: 16785-16790, 2008.
Hochberg LR, Serruya MD, Friehs GM, Mukand JA, Saleh M, Caplan AH, Branner A, Chen D, Penn RD, and Donoghue JP. Neuronal ensemble control of prosthetic devices by a human with tetraplegia. *Nature* 442: 164-171, 2006.
Jackson A, and Fetz EE. Compact movable microwire array for long-term chronic unit recording in cerebral cortex of primates. *J Neurophysiol* 98: 3109-3118, 2007.
Jog MS, Connolly CI, Kubota Y, Iyengar DR, Garrido L, Harlan R, and Graybiel AM. Tetrode technology: advances in implantable hardware, neuroimaging, and data analysis techniques. *J Neurosci Methods* 117: 141-152, 2002.
Johnson JL, and Welsh JP. Independently movable multielectrode array to record multiple fast-spiking neurons in the cerebral cortex during cognition. *Methods* 30: 64-78, 2003.
Kipke DR, Vetter RJ, Williams JC, and Hetke JF. Silicon-substrate intracortical microelectrode arrays for long-term recording of neuronal spike activity in cerebral cortex. *IEEE Trans Neural Syst Rehabil Eng* 11: 151-155, 2003.
Lei Y, Sun N, Wilson FA, Wang X, Chen N, Yang J, Peng Y, Wang J, Tian S, Wang M, Miao Y, Zhu W, Qi H, and Ma Y. Telemetric recordings of single neuron activity and visual scenes in monkeys walking in an open field. *J Neurosci Methods* 135: 35-41, 2004.
Luppino G, Matelli M, Camarda RM, Gallese V, and Rizzolatti G. Multiple representations of body movements in mesial area 6 and the adjacent cingulate cortex: an intracortical microstimulation study in the macaque monkey. *J Comp Neurol* 311: 463-482, 1991.
Matsuzaka Y, Aizawa H, and Tanji J. A motor area rostral to the supplementary motor area (presupplementary motor area) in the monkey: neuronal activity during a learned motor task. *J Neurophysiol* 68: 653-662, 1992.
McCreery D, Lossinsky A, Pikov V, and Liu X. Microelectrode array for chronic deep-brain microstimulation and recording. *IEEE Trans Biomed Eng* 53: 726-737, 2006.
Mitz AR, and Wise SP. The somatotopic organization of the supplementary motor area: intracortical microstimulation mapping. *J Neurosci* 7: 1010-1021, 1987.
Nichols AM, Ruffner TW, Sommer MA, and Wurtz RH. A screw microdrive for adjustable chronic unit recording in monkeys. *J Neurosci Methods* 81: 185-188, 1998.

Nicolelis MA, Dimitrov D, Carmena JM, Crist R, Lehew G, Kralik JD, and Wise SP. Chronic, multisite, multielectrode recordings in macaque monkeys. *Proc Natl Acad Sci USA* 100: 11041-11046, 2003.
Nordhausen CT, Maynard EM, and Normann RA. Single unit recording capabilities of a 100 microelectrode array. *Brain Res* 726: 129-140, 1996.
Otto KJ, Johnson MD, and Kipke DR. Voltage pulses change neural interface properties and improve unit recordings with chronically implanted microelectrodes. *IEEE Trans Biomed Eng* 53: 333-340, 2006.
Pasupathy A, and Miller EK. Different time courses of learning-related activity in the prefrontal cortex and striatum. *Nature* 433: 873-876, 2005.
Pennartz CM, Berke JD, Graybiel AM, Ito R, Lansink CS, van der Meer M, Redish AD, Smith KS, and Voorn P. Corticostriatal Interactions during Learning, Memory Processing, and Decision Making. *J Neurosci* 29: 12831-12838, 2009.
Pesaran B, Nelson MJ, and Andersen RA. Free choice activates a decision circuit between frontal and parietal cortex. *Nature* 2008.
Rivlin-Etzion M, Marmor O, Heimer G, Raz A, Nini A, and Bergman H. Basal ganglia oscillations and pathophysiology of movement disorders. *Curr Opin Neurobiol* 16: 629-637, 2006.
Siapas AG, Lubenov EV, and Wilson MA. Prefrontal phase locking to hippocampal theta oscillations. *Neuron* 46: 141-151, 2005.
Sommer MA, and Wurtz RH. Brain circuits for the internal monitoring of movements. *Annu Rev Neurosci* 31: 317-338, 2008.
Sommer MA, and Wurtz RH. Composition and topographic organization of signals sent from the frontal eye field to the superior colliculus. *J Neurophysiol* 83: 1979-2001, 2000.
Stice P, and Muthuswamy J. Assessment of gliosis around moveable implants in the brain. *J Neural Eng* 6: 046004, 2009.
Strick PL, and Preston JB. Two representations of the hand in area 4 of a primate. I. Motor output organization. *J Neurophysiol* 48: 139-149, 1982.
Sun NL, Lei YL, Kim BH, Ryou JW, Ma YY, and Wilson FA. Neurophysiological recordings in freely moving monkeys. *Methods* 38: 202-209, 2006.
Suner S, Fellows MR, Vargas-Irwin C, Nakata GK, and Donoghue JP. Reliability of signals from a chronically implanted, silicon-based electrode array in non-human primate primary motor cortex. *IEEE Trans Neural Syst Rehabil Eng* 13: 524-541, 2005.
Swadlow HA, Bereshpolova Y, Bezdudnaya T, Cano M, and Stoelzel CR. A multi-channel, implantable microdrive system for use with sharp, ultra-fine "Reitboeck" microelectrodes. *J Neurophysiol* 93: 2959-2965, 2005.
Velliste M, Perel S, Spalding MC, Whitford AS, and Schwartz AB. Cortical control of a prosthetic arm for self-feeding. *Nature* 453: 1098-1101, 2008.
Vetter RJ, Williams JC, Hetke JF, Nunamaker EA, and Kipke DR. Chronic neural recording using silicon-substrate microelectrode arrays implanted in cerebral cortex. *IEEE Trans Biomed Eng* 51: 896-904, 2004.
Ward MP, Rajdev P, Ellison C, and Irazoqui PP. Toward a comparison of microelectrodes for acute and chronic recordings. *Brain Res* 2009.

Yamamoto J, and Wilson MA. Large-scale chronically implantable precision motorized microdrive array for freely behaving animals. *Journal of neurophysiology* 100: 2430-2440, 2008.

TABLES

Monkey ID	G	Y	H	J	K	L	M	Overall
Chamber lifetime (yrs)	3.2	4.6	3.0	3.7	2.2	2.5	4.5	3.4
Implant duration (days)	189.5	265	121	264	36.3	53	40.5	130.9
Brain areas targeted	7	6	14	10	4	4	6	7.3
Implanted electrodes	84	87	119	115	38.7	39	36	74.8
Recording sessions	75	101.5	24	28	18	20.5	17.5	38.1
Unit-recording electrodes (total)	2196	1816.5	696	723	411	359	253	875.9
Yield:								
1st day of recording	50%	30%	35%	22%	30%	17%	24%	30%
Maximum	60%	36%	39%	32%	79%	78%	71%	57%
Minimum	24%	8%	10%	12%	21%	8%	24%	15%
Mean across all recording sessions ± s.d.	35% ±10%	21% ±6%	25% ±7%	23% ±7%	56% ±17%	47% ±21%	43% ±18%	31% ±16%
Mean unit-recording electrodes per session	29	19	29	25	21	19	18	23
Unit-recording electrodes with activity on at least one day	83%	81%	82%	67%	77%	73%	71%	77%

Table 1 | Summary of implant statistics. Values for each monkey were averaged across implants. Overall values were calculated from grand averages across all monkeys and implants.

FIGURE CAPTIONS

FIG. 1. Reconfigurable chronic electrode implant system. *A*: Exploded-view schematic of chamber cap, microdrives (left to right, 9, 6, or 3 screws for driving electrodes), grid, connector strips and chamber. Side ports in the chamber below the level of the grid provide access for cleaning and observation of the granulation tissue over the dura. A ridge along the top of the chamber prevents fluid from contaminating the microdrives and connector strips. The chamber cap has upper slots for ventilation and removable side panels for easy access to the connector strips. *Inset*: a three-screw microdrive loaded with a single electrode. A beveled 27-gauge guide-tube is used for punching through the dura mater and fits inside a shorter 23-gauge tube to minimize friction with the grid hole. *B*: Top- and front-views of a non-loaded three-screw microdrive. Electrodes can be glued to the slotted plastic sled attached to each screw. When the screw is turned, the plastic sled moves along the screw shaft, guiding the attached electrode through a grid hole immediately adjacent to the row of grid holes covered by the drive itself, thereby maximizing the number of grid holes that can be targeted simultaneously in a single implant. *C*: Top-view of 117 electrodes in monkey H (implant 1). Insulating varnish is red. Black, red, yellow, and gray wires are the leads from tubes used for reference. *D*: Front-view of an implant of 111 electrodes in monkey J. On the sides, five preamplifiers are connected to the electrode leads via black connector strips. White silicone covers the surface of the grid at the base of the microdrives to promote dryness above the grid. Reference wires, ground wires, and the exposed surfaces of pins are insulated with paint. The depth of each electrode can be manipulated independently by turning the appropriate microdrive screw with a small flat-head screwdriver. *E*: A six-screw microdrive with a

conventional tungsten microelectrode glued to the plastic sled on each screw. All scale bars, 1 cm.

FIG. 2. Localization of electrodes simultaneously implanted in cortical and subcortical structures. *A*: Coronal section from a T2-weighted structural MR image of monkey D showing the saline-filled grid and chamber above granulation tissue covering the intact dura mater. *B*: Dorsal view of right hemisphere of monkey J's brain (anterior at top, medial wall at left). Scale bar, 1 cm. *C*: Coronal cresyl violet-stained section from monkey H showing tracks of three electrodes targeting the CN (left) and a fourth approaching the Put (right), all from implant 3, which was removed after the monkey was perfused. Note the remarkably straight approach to the deep targets. *D*: Coronal cresyl violet-stained section from monkey G showing tracks of electrodes that recorded from the CN (lower arrow) and dlPFC (upper arrow) in implant 2. Scale bar, 1 cm.

FIG. 3. Simultaneously recorded neural activity from multiple cortical and subcortical sites. *Center*, top-down view of macaque brain showing configuration of electrodes implanted in one hemisphere of each of two chronic implants (left, monkey H, implant 3; right, monkey G, implant 1; both monkeys were implanted bilaterally, but for purposes of visualization, only one hemisphere is shown for each monkey). Black lines identify the recording sites (projected onto the brain surface) for each sample neural signal shown. *Left column*, spectrograms of LFP power simultaneously recorded from example sites on day 159 of the implant, during joystick task performance. Spectrograms are aligned in windows on the following task events: trial start (E), cues onset (C), 1^{st}-3^{rd} joystick

movement onset (M1-3) and reward delivery (R). The brain structure and electrode number are listed above each spectrogram (abbreviations as in main text). Power at each frequency indicated by color ranging from blue (-5 dB) to red (5 dB). *Right column*, feature plots and average waveforms of units simultaneously recorded from the example sites on implant day 126, during performance of an oculomotor scan task. Feature plots show first principal component vs. peak-valley amplitude. Average waveforms are 1 ms in duration and shading indicates ±3 s.d.

FIG. 4. Sampling at different depths across recording sessions. *A*: Three-dimensional schematic of all recording tracks for the duration of a single chronic bilateral implant (monkey H, implant 3, 172 days). Medial wall (left) and dorsal surface (right) of cortex shown in gray. Approximate locations of the CN (dark gray) and Put (light gray) also indicated. Vertical colored lines represent the trajectories of the tips of the electrodes from the first through the last recording session of the implant. Dots indicate the electrode tip locations in a recording session midway through the course of the implant (day 98). Color of each line indicates targeted brain structure. *B*: Spectrograms of LFP power recorded from two electrodes (labeled 1 and 2 in left hemisphere of **a**) in four sessions at four depths. Spectrograms follow same conventions as in Fig. 3. Day of implant, session-to-session change in depth and brain structure shown for each recording site (s, m, d indicate superficial, middle and deep layers of cortex, respectively). *C*: Peri-event time histograms of single-unit spiking activity recorded in three sessions at three depths from an electrode targeting the CN in the right hemisphere (monkey G, implant 1, oculomotor scan task, in which monkeys freely scanned visual targets to find the baited

one). Each row shows data from a single session and recording depth (implant day, number of trials and change in depth shown).

FIG. 5. Mean yield over time across implants. The fraction of electrodes that recorded unit activity out of the total number of electrodes averaged over 16 implants in seven monkeys. All electrodes were implanted in the brain on day 0. As not all implants have a yield measurement for each day of the implant (see Fig. 6), the mean yield (± s.e.m.) is shown for the pool of available data in five-day bins.

FIG. 6. Yield of individual implants across recording sessions. The fraction of electrodes with recorded unit activity out of the total number of electrodes in each of 16 total implants. All electrodes were implanted in the brain on day 0. Vertical scales in the left column (*A-H*) are half of those in the right column (*I-P*), in order to better illustrate differences in yield over time for those implants that had a lower maximum yield. The shorter and smaller implants had higher maximum yields.

FIG. 7. Yield of new and existing units across recording sessions. *A-C*: For each session of implants 1-3 of monkey H, the fraction of electrodes that recorded unit activity and had recorded unit activity in the preceding recording session is shown in red (existing units). Also shown are the fractions of all electrodes that recorded new unit activity and that either had been moved since the preceding recording session (new units with moving, blue) or had not (green). All electrodes were implanted in the brain on day 0. *D*,

E: Same as *A-C*, except that the electrodes recording new unit activity have not been subdivided into moved vs. not-moved since the preceding session.

FIG. 8. Session-to-session stability of neural recordings. *A*: Day of implant, mean wave shape (± 3 s.d.) with inset of first principle component vs. peak-valley feature plot, autocorrelogram and PETH aligned on visual targets on (green line) for a single electrode targeting the CN in the chronic implant of monkey G during performance of the oculomotor scan task. Each row corresponds to a different recording session. Electrode was moved between day 88 and 106 and again between day 115 and 128. The reduction in phasic unit firing in the PETH on day 111 may be due to the introduction of a new visual task on that day. *B*: Spectrograms from an electrode in the dlPFC of monkey H (implant 2) during performance of the joystick task. Aligning events are the same as in Fig. 3. Responses from the middle layers of area 9/46 are shown in recording sessions spanning 92 days. Electrode was moved to the deeper layers of 9/46 between day 120 and 139.

FIG. 9. Cortico-cortical connectivity demonstrated by electrical stimulation in ACC. Rasters and histograms of the spiking activity of single units recorded simultaneously from eight chronically implanted electrodes in the cingulate cortex during 500 stimulation trials (bin width, 0.1 ms). Electrical stimuli were delivered between two chronically implanted electrodes in the ACC (anode and cathode indicated by + and -). Of the 15 units simultaneously recorded in the ACC and CMA, seven units showed

significant responses to the stimulation (beyond the 99% confidence limits estimated from the pre-stimulation baseline firing rates) within 5 ms of the stimulus.

FIG. 10. *A*: Selective modulation of LFPs in CN by electrical stimulation in dlPFC. For each of four stimulation locations in dlPFC, averages of LFP waveforms recorded simultaneously from eight electrodes chronically implanted in the CN are shown, aligned on the onset of stimulation (40 trials; blue shading, 95% confidence intervals). Different striatal sites exhibited significant modulation, depending on the stimulation site in dlPFC. *B*: Localized neural effects of a subcortical pharmacological injection. The firing rates of simultaneously recorded neurons in the dlPFC (top) and head of the CN (bottom) are shown aligned on the onset time of drug injection in the CN (vertical black line), using the ChIME system. The striatal, but not prefrontal, units exhibited significant changes in firing rate (pink shading) after drug infusion, in comparison to average pre-drug activity. Scale bar, 2 min.

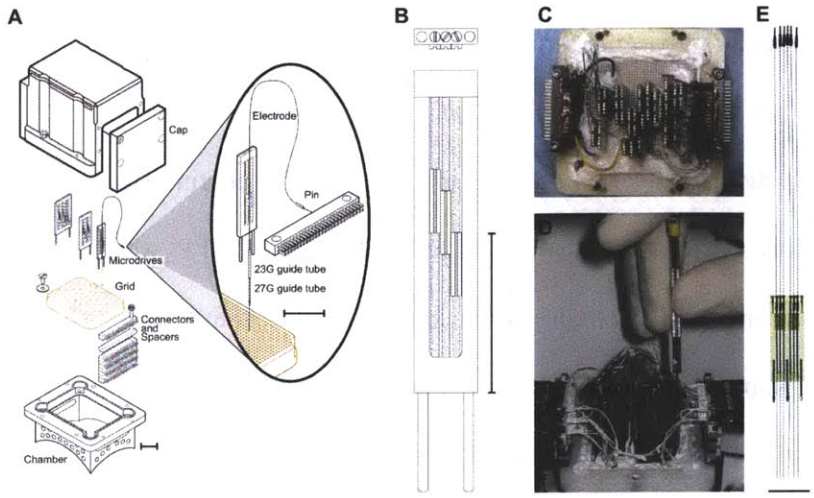

Figure 1 - Graybiel

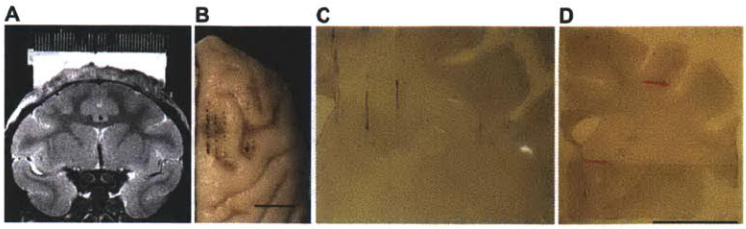

Figure 2 - Graybiel

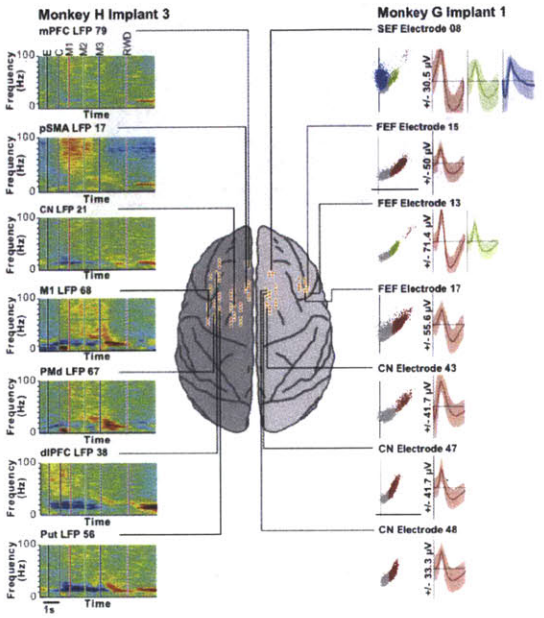

Figure 3 - Graybiel

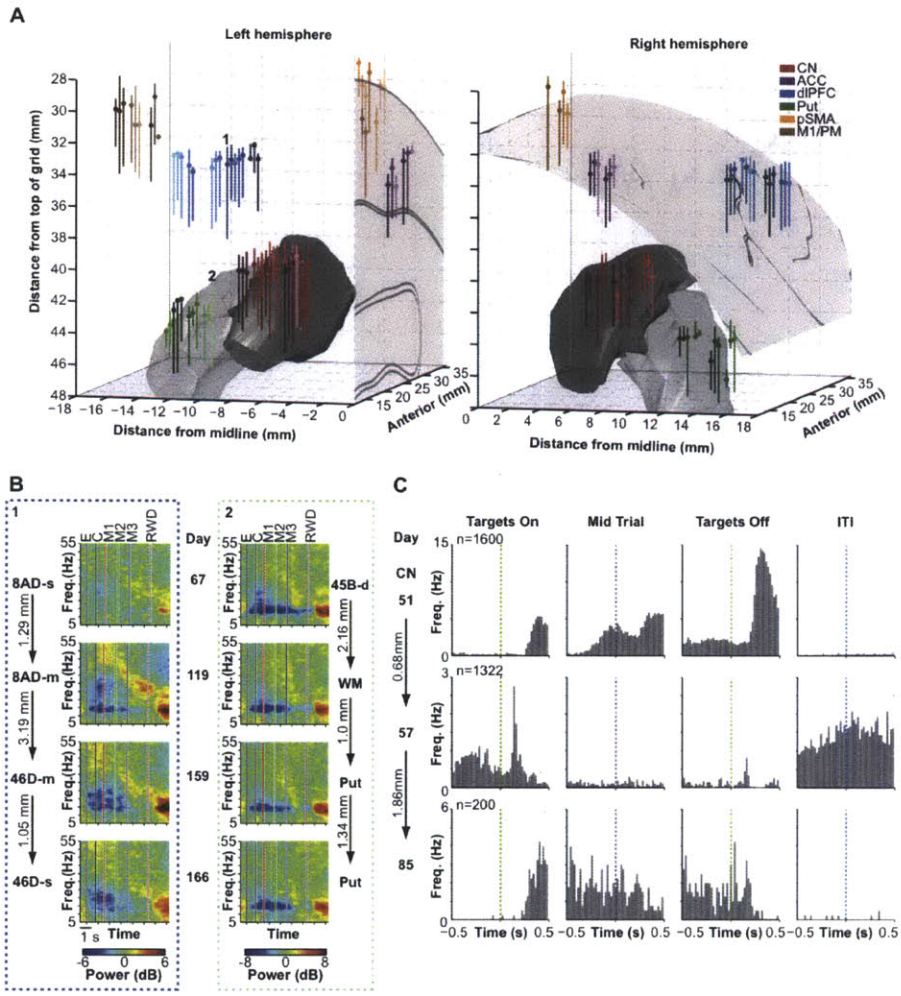

Figure 4 - Graybiel

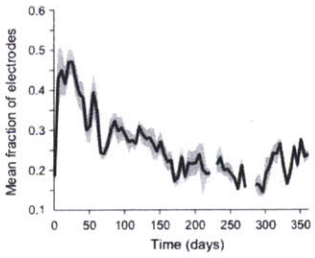

Figure 5 - Graybiel

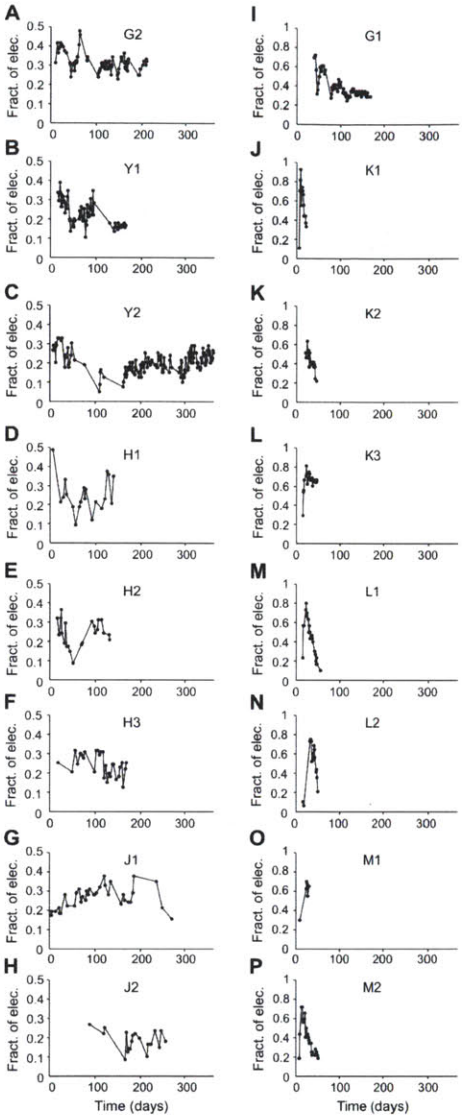

Figure 6 - Graybiel

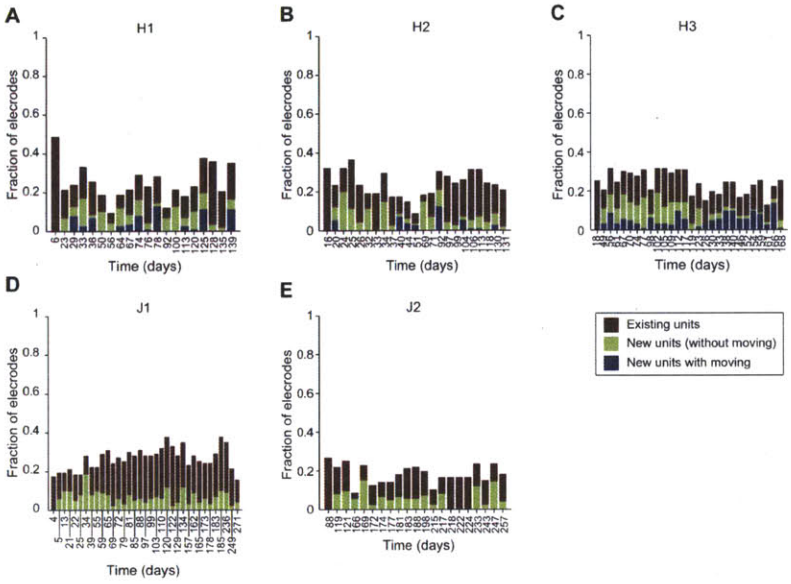

Figure 7 - Graybiel

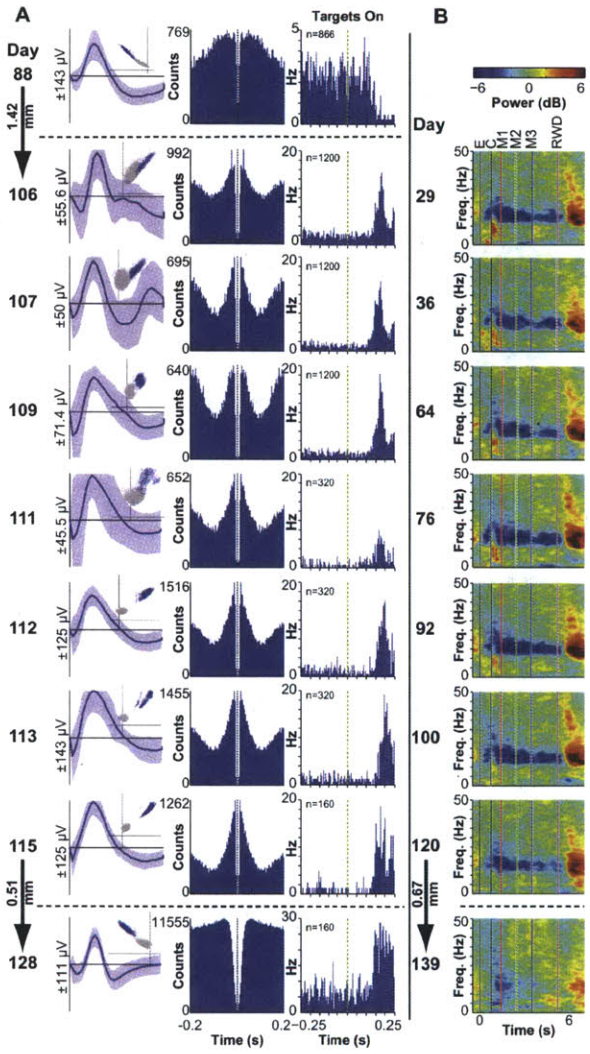

Figure 8 - Graybiel

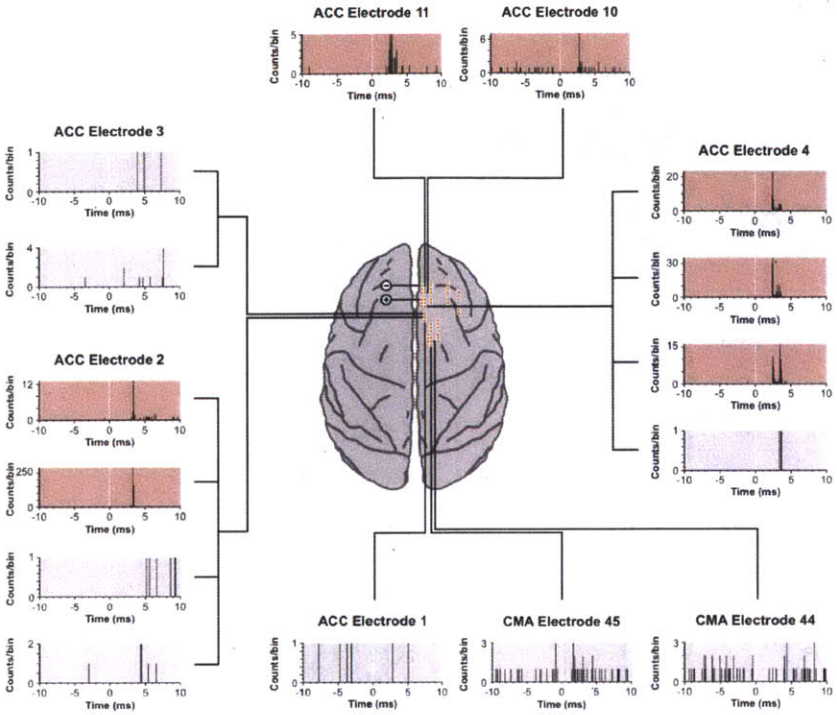

Figure 9 - Graybiel

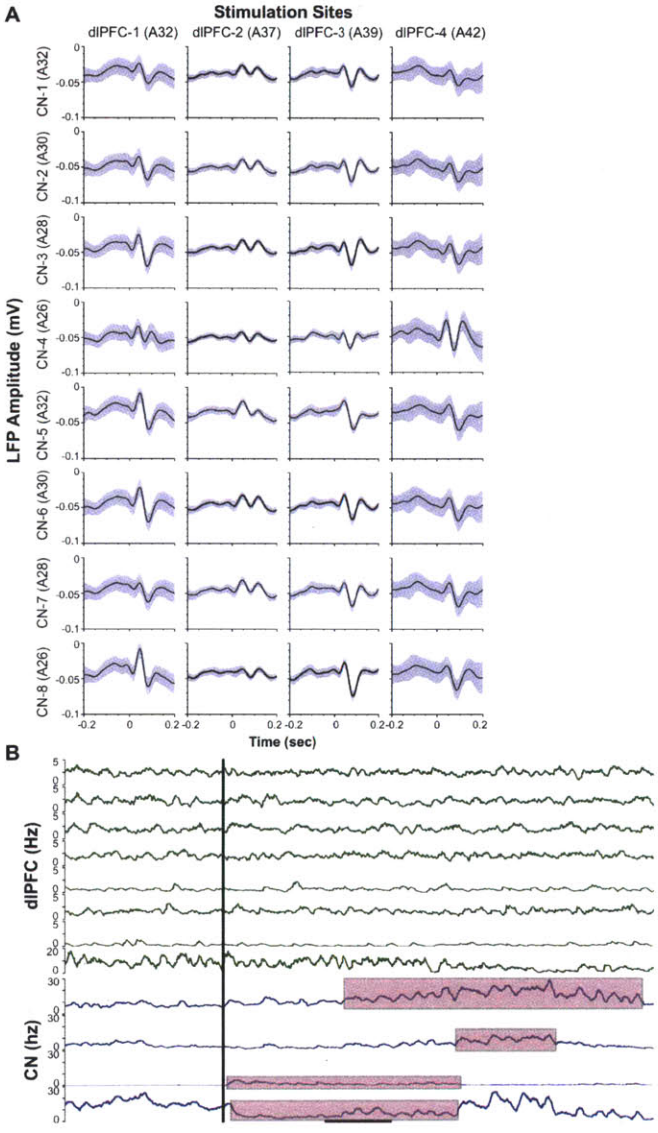

Figure 10 - Graybiel

CHAPTER III

Beta oscillations in frontal cortex and striatum represent post-processing of successful behavior

Joseph Feingold[1,2], Daniel J. Gibson[2] and Ann M. Graybiel[2,3]

[1]HST, MIT, Cambridge, MA, USA

[2]MIBR, MIT, Cambridge, MA, USA

[3]BCS, MIT, Cambridge, MA, USA

ABSTRACT

Excessive beta band (13-30 Hz) activity in cortico-basal ganglia circuits is a pathophysiological signature of Parkinson's disease. Yet, the function of beta oscillations in the diseased or healthy primate brain is not clear. Current theories link beta activity to idling or the preservation of the current state of cortical areas. Here we show that beta oscillations in the local field potentials in frontal cortex and striatum of monkeys performing arm movements were not directly related to movement, but to the offset of behavioral performance. In all brain regions, beta oscillations occurred in brief, spatially localized bursts that were most pronounced following movement or task performance. Beta bursts were detected based on their relative contribution to the spectrum of the LFP signal, as opposed to their overall amplitude. The rates and power of beta bursts differed across brain regions. Post-performance beta burst rates and power tracked the details of the preceding task performance, with different details driving the rates differently by brain region. In striatum and prefrontal cortex, beta burst rates were higher following correct trials than errors, and the bursts at pairs of sites across these regions were coherent. Based on our results, we propose that beta oscillations represent post-performance reinforcement of the network activity that led to the desired behavioral outcome obtained immediately prior.

Oscillations in the beta frequency (13-30 Hz) range in sensorimotor cortex have long been associated with movement. The hallmark of beta activity in cortical motor areas is a pattern of peri-movement suppression (relative to rest) followed by post-movement rebound. This pattern has been observed in local field potential (LFP) and EEG recordings from cortical motor areas in humans[1] and monkeys[2-4] performing simple single or repetitive movements, such as finger presses or wrist movements. Typically, beta activity falls to a minimum following cue presentation or movement execution, and reaches a maximum immediately following movement. In view of this pattern, beta was labeled an "idling" frequency[5], with beta band oscillations theoretically representing a minimal energy state that the brain enters in the absence of processing.

The finding of pathologically excessive beta band synchrony in patients with Parkinson's disease (PD) and animal models of Parkinsonism[6] has fueled renewed interest in the potential role of beta oscillations in healthy and abnormal brain function. While the clinical consequences of elevated beta synchrony are not clear, evidence has been mounting that it can be reduced by the leading treatments for PD[7,8]. Recent studies have also shown that decreases in beta activity in the subthalamic nucleus can correlate with decreases in motor symptoms of PD, specifically bradykinesia (slowness of movement) and rigidity[9]. Other work[10] recently established a link between high cortical beta power and bradykinesia, and some have proposed that the benefits of deep-brain stimulation therapy are mediated by reducing high beta synchrony[11]. Patients with PD typically present with cognitive[12,13] symptoms, in addition to motor ones, though it is not clear how beta

synchrony, or its potential reduction by therapy, might be related to non-motor symptoms.

Based on the mounting evidence implicating beta activity in PD, a recent theory proposed that, rather than represent neuronal idling, beta oscillations (or the mechanisms that give rise to them) might actively gate movement[14]. The putative inverse relationship between high beta activity and movement is complicated by the increase in beta activity observed in healthy subjects during sustained motor output, including the maintenance of a precision grip[15] or the application of a constant force[16]. These findings support the notion of beta activity representing not the absence of motor output, but rather a decreased likelihood of changing the existing motor output[17]. More recently, this connection between beta activity and preserving the status quo was extended to cognitive processes by Engel and Fries[18], who proposed that the role of beta oscillations in brain regions involved in cognitive processing is to preserve the current state. According to this idea, beta oscillations in a given brain region should be higher when that region does not anticipate an impending change in output or set.

Despite their theoretical appeal, none of these interpretations of beta activity (idling, anti-kinetic or preserving the status quo) fits well with the core phenomenon of maximal beta activity occurring in cortical motor areas immediately following movement. If beta activity reflects idling or conservation of the current state or output, why is it highest following movement, but relatively low during rest (behavioral "idling")? We hypothesized that the prominent post-movement rebound in beta power is a ubiquitous signature of active post-performance processing in the brain. The role of such post-processing might be to facilitate cross-structure coordination of neuronal

activity related to the preceding performance and its outcome, which are required for mechanisms of synaptic plasticity. To test this hypothesis we analyzed LFPs recorded simultaneously from multiple cortico-striatal regions in the monkey brain, known to be directly involved in motor control, movement sequencing and executive function[19-22]. In order to discover the potential role of beta activity in movement behavior, we trained the monkeys to perform a comprehensive set of behavioral tasks, focused largely on sequences of movements, which to date have not been used to study systematically the modulation of beta activity. We found that, in all tasks, LFPs in frontal cortex and striatum were characterized by brief, spatially localized episodes, during which beta frequencies disproportionately dominated the LFP spectrum. These beta bursts were most pronounced following behavioral performance, when they were modulated by specific features of the preceding behavior, and, in striatal and prefrontal sites, also by the outcome of that behavior. Based on our results, we propose that the role of beta oscillatory activity might not be to preserve the current state or behavioral output of individual brain regions, but to preserve or reinforce the cortico-striatal network dynamics that led to the desired outcome obtained immediately prior.

Prominent post-performance beta oscillations

In order to record LFPs simultaneously from multiple cortical and subcortical regions of the monkey brain, we developed a novel method for chronically implanting large numbers of independently moveable micro-electrodes (see Chapter 2 of this thesis). Using this system, we recorded LFPs from hundreds of sites in primary motor and dorsal premotor cortex (M1PMC; combined because the results were similar), dorsolateral

prefrontal cortex (dlPFC), caudate nucleus (CN) and putamen (Put) of two Rhesus monkeys. The monkeys had been trained extensively to perform single and sequential joystick movements in response to visual cues (Fig. 1a, 1M1T and 3M3T tasks, respectively). Each movement was preceded by a short or long hold period (as indicated by the shape of the preceding visual cue), which the monkeys had to self-time accurately. The monkeys performed the behavioral tasks in order to obtain a liquid reward (of constant amount across trials of all tasks), the delivery of which was contingent upon the correct completion of the trial.

In all brain regions, the trial-averaged power in the beta band recorded at each site was suppressed during the cue and movement periods (Figs. 1b and S1) relative to rest (defined as the average value of the beta power recorded at each site during prolonged rest periods (Fig. 1b, dashed lines) before and after behavioral task performance). In M1PMC, the trial-averaged beta power during the 1M1T task reached a maximum immediately following the offset of the movement (Fig 1b, thin arrows). Interestingly, the highest peak in beta power during the 3M3T task occurred following the offset of the last movement in the sequence, not following each movement. Additional minor peaks were observed following the first and second movements, but only during long hold periods. Thus, the peak in beta power in M1PMC was not locked to the offset of any given movement *per se*, but rather to the offset of the *last* movement in a sequence. This suggests that beta activity in M1PMC may be related to the completion of, and subsequent disengagement from, the performance of a motor task.

The timing of the rebound in power in dlPFC and striatum was dramatically different from what it was in M1PMC. Instead of peaking in the post-movement period,

as in M1PMC, beta power in dlPFC and striatum peaked in the post-trial period, following reward delivery and the subsequent offset of the visual cues (Fig 1b, thick arrows). This difference in the timing not only shows that beta activity was different between M1PMC and the other brain regions, but further demonstrates that beta activity was not simply locked to movement onset or offset.

Our results argue against a simple relationship between movement and the modulation of beta activity, even in M1PMC. Nevertheless, they were obtained during the performance of tasks requiring overt motor responses. Does the suppression-rebound pattern of modulation in beta power occur only during trials involving movement? To answer this question, we analyzed the timing of the peaks in beta power during trials of a third task, 0M3T, in which the monkeys were presented with the same visual cues as in the 3M3T task (Fig. 1a), but were required to withhold movement in order to obtain reward (see Methods). Remarkably, in the 0M3T task, the beta power in each of the four brain regions exhibited a pattern of peri-cue suppression, followed by a rebound during the post-trial period (Supplementary Fig. 1).

Bursts of spatially localized beta activity

The time-course of the trial-averaged beta power in relation to task performance suggests the existence of sustained beta oscillations either post-movement (in M1PMC) or post-trial (in dlPFC and striatum). Sustained oscillations, if present during periods of rest or "steady-state" behavior, would support current interpretations of beta activity as an indicator of idling or of state-preserving processes. However, our results so far have been based on trial averages. In order to detect the occurrence of sustained beta oscillations

during task performance, we analyzed individual trials. Much to our surprise, no single trial resembled the trial average, in that there were no periods of sustained high-amplitude beta oscillations. Rather, each trial was characterized by brief (~150 ms) episodes during which beta frequency oscillations dominated the spectrum (Fig. 2a). These bursts of oscillations in the beta band were detected based on their relative contribution to the spectrum of the LFP signal, as opposed to their overall amplitude. In each brain region, beta bursts occurred throughout the trial, even during movements. However, the modulation of the burst rate in each region closely followed the modulation of the trial-averaged beta power in that region (Fig. 2b). This led us to reinterpret the trial-averaged beta power as expressing the time-dependent probability in any given trial that a beta burst will occur. The large trial-to-trial variability in burst amplitude and duration, as well as in the timing of the bursts relative to task events, gives rise to the temporally extended peaks in the trial-averaged power.

Beta oscillations were not only temporally discrete, but were also localized in space. To analyze this, we computed the cross-covariance between the envelopes of beta bursts recorded at pairs of sites. In each of the four brain regions we studied, the peak cross-covariance decreased significantly as the distance between the recording sites increased (Fig. 2c; unless otherwise noted, statistical significance was assessed using an ANOVA corrected for multiple comparisons, alpha = 0.05). The degree to which bursts were spatially localized differed across brain regions, with dlPFC exhibiting significantly greater localization of bursts than M1PMC and the striatum for distances of 1.5 mm or more between paired sites. The differences between regions in the spatial localization of bursts can be seen in individual trials, by comparing the bursts across the population of

simultaneously recorded sites across the four brain regions (Supplementary Fig. 2). Importantly, the phase of the coherence between bursts in the LFPs from even the closest pair of simultaneously recorded electrodes in the CN was significantly different from zero (Supplementary Fig. 3), arguing against the possibility that electrotonic volume conduction between the sites could have accounted for the high cross-covariance observed between bursts. Our results demonstrate that cortical and striatal beta activity occurs in the form of spatiotemporally discrete episodes, the modulation of which varies from trial to trial and from site to site.

We found no evidence for waxing and waning beta oscillations, but rather, a time-dependent probability of beta burst occurrence that varied by brain region (Fig. 3a, 1M1T and 3M3T tasks). For each site, we calculated the rate of bursts in each task period relative to the average rate during rest periods at that site, and averaged the rates across all sites within each brain region. The modulation of the population average burst rates in each brain region followed the time-course of the trial-averaged beta band power in all behavioral tasks (Fig. 3a; compare to Fig. 1b). During the cue and movement periods, beta burst rates were suppressed relative to the average value during rest periods. The rest-normalized burst rates then peaked in M1PMC post-movement, whereas in dlPFC and striatum, the burst rates peaked post-*trial*. The population average burst power (normalized to rest) followed a similar pattern of modulation across task epochs (Supplementary Fig. 4a). In addition to the burst rates that were normalized to rest, we examined the modulation of the absolute burst rates (Supplementary Fig. 4b). Although the highest normalized bursts rates in the post-trial period were in the dlPFC, this region showed the lowest absolute burst rates. The converse was true of the M1PMC bursts.

Thus, across brain regions, there was an inverse relationship between the rate of bursts during rest and the degree to which those rates changed following trial performance.

We tested whether beta burst rates and power during the post-trial period were modulated by specific aspects of the preceding trial. For this purpose, we added a fourth behavioral task, 1M3T, in which the monkeys were presented with the same visual cues as in the 3M3T task, but were required to perform only the first instructed movement in order to obtain reward. We compared the rate and, separately, the power, of beta bursts following trials of four behavioral tasks (performed in separate blocks of each experimental session; performance rates were similar across all tasks), involving different numbers of movements (0M3T, 1M3T and 3M3T) or of visual cues indicating the potential spatial targets of movement (1M1T and 1M3T). In each brain region, the population average of normalized rates of beta bursts in the post-trial period were modulated significantly by the details of the preceding behavioral task performance (Fig. 3b-e, asterisks indicate significant differences between burst rates in adjacent tasks). The population average of normalized beta burst power in the post-trial period matched the pattern of burst rate modulation across tasks (Supplementary Fig. 4a, right-most panel).

Not only were the post-trial burst rates modulated by the preceding trial type, but the pattern of modulation differed across brain regions. In M1PMC, burst rates showed significant modulation between tasks with 0, 1 or 3 movements, regardless of the number of visual targets (Fig. 3b). Thus, the rate of bursts in M1PMC during the post-trial period tracked the number of movements that the monkey had performed in the preceding trial. This is surprising given that beta activity (both rate and power) in M1PMC during this time period was below the peak levels attained during the immediate post-movement

period, and was, in fact, close to rest levels. In contrast to these burst patterns in M1PMC, the pattern of beta burst rate modulation in CN and Put during the post-trial period across different tasks indicated a significant effect of the number of visual cues, as opposed to the number of movements, in the preceding trial (Fig. 3c, d). This relationship between striatal burst rates and the number of visual cues was consistent so long as the monkey was performing a movement task, as opposed to withholding movement (in the 0M3T task). Finally, the burst rates in dlPFC increased with increasing numbers of movements and of visual cues instructing movement (Fig. 3e). Importantly, individual LFPs in each brain region exhibited patterns of task-dependent modulation of post-trial burst rates that were qualitatively similar to the patterns found for the population averages (Supplementary Fig. 4c-f, thin lines). This agreement between the results for individual LFPs and those for the population average confirms that post-trial bursts in localized sites in each brain region were modulated by the same aspects of the preceding behavioral task performance that modulated the population average burst rates.

To determine whether the post-trial burst rates depended on the outcome of the trial, we tested whether beta burst rates following correct trials differed from those following error trials (Fig 3b-e, solid thick vs. dashed thin lines, respectively). In order to control for possible differences in the number of movements between correct and error trials, we focused on the single-movement tasks, and analyzed only those error trials in which the monkey had performed a single movement (the monkeys could have made a movement that resulted in an error trial either by initiating the movement too quickly or by making the movement in an incorrect direction; min. of 20 error trials per condition). In dlPFC and striatum, the burst rates following error trials were significantly lower than

those following correct trials (Fig. 3c-e, solid vs. dashed lines). In contrast to the other brain regions, the burst rates in M1PMC following error trials were significantly higher than those following correct trials. In fact, the burst rates in M1PMC following error trials were indistinguishable from those in the post-movement period in correct trials. This is not surprising, given that, in terms of the timing relative to the offset of movement, the post-trial period following error trials coincided with what would have been the post-movement period in correct trials. This fact indicates that, unlike striatum and dlPFC, the M1PMC burst rates in the post-trial period were not modulated by the overall outcome of task performance.

Temporal relationships between beta bursts

Given that, in all tasks, the rate and power of beta bursts in the dlPFC and striatum were highest during the post-trial period, we asked whether during this period the bursts at pairs of striatal-prefrontal sites exhibited consistent temporal relationships. We found that they did, both in terms of the co-occurrence of bursts at pairs of sites and the beta band coherence during co-occurring bursts. First, we computed the cross-covariance between each pair of simultaneously recorded LFPs in the CN and dlPFC. The average lag of the peaks in the cross-covariance across all CN-dlPFC pairs was indistinguishable from zero, demonstrating that bursts tended to co-occur across the paired CN and dlPFC sites. Second, we analyzed the coherence between the same LFP pairs. We found that the population-average LFP-LFP coherence reached a peak at beta frequencies during the post-trial period, following trials of the 1M1T and 3M3T tasks (Fig. 4a, c). The coherence values at these post-trial peaks were significantly higher than the coherence in

any other trial period. Given the prominent bursting at beta frequencies during the post-trial period, we asked whether the high coherence during this period might be due to elevated coherence specifically between beta bursts. Indeed, individual pairs of recording sites in the CN and dlPFC showed significantly higher post-trial coherence during periods in which both LFPs were bursting, than when neither was bursting (Fig. 4b, d). The significantly non-zero phases of the coherence in either case rules out the possibility of volume conduction between the two sites or from a common third site. At the population level, the magnitudes of the coherence among pairs of LFPs that were bursting was ~3 times greater than the magnitudes of the coherence of paired LFPs that were not bursting. The ratio of LFP-LFP coherence during bursts vs. non-bursts was significantly higher during the post-trial period in all tasks than during rest periods. Moreover, the ratio differed significantly across tasks, and was inversely related to the number of movements performed in the preceding trial. In summary, the largely co-occurring post-trial beta bursts in the CN and dlPFC were highly coherent, in a task-dependent manner.

In addition to the temporal relationships between bursts in different brain regions, we studied the co-activation of bursts across different sites within each region. These results are preliminary, based on data from a single experimental session. Our analysis took into account the entire population of simultaneously recorded LFPs within each region, as opposed to averaging results across all pairs of LFPs. Beta bursts in the striatum were significantly more co-active than beta bursts in M1PMC and dlPFC. This fits well with the earlier results of the cross-covariance between bursts at pairs of increasingly distant sites (Fig. 2c), as well as examples of bursts across the population of simultaneously recorded sites in individual trials (Supplementary Fig. 2). In M1PMC and

striatum, the co-activation of bursts in the post-trial period (normalized to the co-activation during rest periods) was modulated across tasks in ways that were similar to the task-modulation of the population average burst rates. The post-trial bursts in dlPFC, in contrast, exhibited a pattern of modulation across tasks that was opposite to the corresponding pattern of burst rate modulation.

DISCUSSION

In order to discover the potential role of beta oscillations in movement behavior, we analyzed the modulation of beta activity in the frontal cortex and striatum of monkeys as they performed a range of behavioral tasks. The timing of peak trial-averaged beta power relative to behavioral events supports a role for beta oscillations in active post-performance processing of behavior. Investigating the source of the peaks in the trial-averaged beta power, we discovered that beta activity was characterized by brief, spatially localized bursts of oscillations, whose rate and power were modulated by the behavioral tasks in a manner similar to the modulation of trial-averaged beta power. The modulation of post-trial bursts by task features (numbers of movements or visual cues) differed across brain regions. Beta bursts in M1PMC were driven primarily by the number of movements in the preceding trial; striatal bursts were driven by the number of cues; and prefrontal bursts were driven by a combination of both. Post-trial beta burst rates in striatum and dlPFC were also modulated by the outcome of the preceding behavioral task performance—burst rates in these brain regions were significantly higher following rewarded correct trials, as opposed to unrewarded errors.

Our finding of packet-like post-performance bursts of beta oscillations across frontal cortex and striatum that were modulated by specific features of the preceding behavior as well as the outcome of that behavior, raises the possibility of cross-structure coordination or communication during beta bursts. Computational work has shown that beta oscillations are particularly well-suited to long-range interactions[23], and recent physiological work has described task-dependent changes in beta coherence across cortical regions[24]. Nevertheless, the degree of beta band coherence between frontal cortex

and striatum in the healthy primate brain is not clear from the literature. We found that, for a majority of the pairs of simultaneously recorded CN and dlPFC sites, the lag time of the peak cross-covariance between the post-trial burst trains was not significantly different from zero, indicating a predominance of co-occurring beta bursts across striatal and prefrontal sites. During the post-trial period, when beta burst rates were typically highest in these brain regions, the average LFP-LFP coherence across all pairs of CN-dlPFC sites reached a maximum in the beta band. Most importantly, LFPs recorded simultaneously at paired sites in CN and dlPFC exhibited increased coherence specifically during overlapping beta bursts. The close temporal alignment of bursts of beta oscillations across CN and dlPFC strongly suggests that these bursts may facilitate communication or coordination of activity across these brain regions.

Taken together, our results lead to a novel unifying interpretation of beta oscillations in the brain. Our findings argue against the prevailing views that beta activity either gates movement execution or prevents brain regions from changing their present activity (and hence, the current behavioral output). Rather, we propose that beta oscillations represent mechanisms for integrating the successful outcome of behavior with the details of the performance that led to that outcome, across cortico-striatal networks. The purpose of such mechanisms could be to increase the likelihood of achieving goals in future trials, in either of two ways—by preventing changes to the network dynamics that led to a rewarded outcome, or by actively reinforcing those network dynamics. The high rate of striatal-prefrontal co-bursting that we found, coupled with the high LFP-LFP coherence, which we observed particularly during co-bursting episodes, can lead to sub-millisecond-scale alignment of neural activity across widely

separated sites in the cortex and striatum. Such precise temporal coordination is required for spike-timing-dependent plasticity {{refs}}, and poses a daunting challenge for distant populations of cells to overcome. Coordinated, coherent bursts of beta oscillations could play a pivotal role in facilitating known mechanisms of learning-induced changes in synaptic connectivity within the fronto-striatal circuitry.

The role we are proposing for beta oscillations is consistent with the leading ideas about their mechanistic origins. In frontal cortex and basal ganglia beta oscillations are thought to arise from the interplay of excitatory and inhibitory feedback[25]. In the basal ganglia specifically, computational work has identified the GPe-STN network as a likely candidate generator of beta oscillations, which can arise from the inhibition of STN by GPe, coupled with the excitation of GPe by the STN[26]. Beta oscillations could thus be viewed as indicators of the finely tuned balance between excitation and inhibition across heterogeneous networks. On this view, co-occurring beta oscillations across different network nodes would be sensitive to any changes in the local excitatory-inhibitory balance. Prominent beta oscillations could be taken as evidence of zero net changes in network connectivity, consistent with a role in preventing plasticity of networks that just led to reward. Alternatively, the high beta activity we observed following correct trials could indicate the excitatory and inhibitory feedback processes involved in the tuning or updating of the fronto-striatal networks in response to the rewarded completion of the task.

Low beta activity following an unrewarded outcome may allow synaptic plasticity to occur, mediated by other mechanisms. The purpose of such plasticity could be to change the network dynamics in order to increase the likelihood that the desired outcome

will be obtained in the future. This would be particularly useful in learning situations (exploration). Support for this idea has recently been found in rat ventral striatum (Howe et al, *PNAS* in press). LFPs in ventral striatum of naïve rats performing an auditory-cued t-maze task, did not exhibit prominent beta activity following reward. As the rats learned the task, beta LFP activity evolved so that it eventually became much more pronounced following correct trials than errors. This is consistent with a role for beta activity in preserving learned behaviors that lead to rewarded outcomes.

If high beta activity is related to network plasticity, the low beta activity we have observed following occasional errors in the performance of well-learned behaviors might prevent the inappropriate reinforcement of the network activity that led to the undesired outcome. In such a scenario, low beta activity would effectively prevent the occasional erroneous performance from modifying the monkey's typically successful behavior. Beta activity would thus maintain the learned network settings by making them less susceptible to change by infrequent errors (exploitation). Thus, rather than promoting the current behavioral output, as suggested by the status quo-preserving theory, beta oscillations could be involved in promoting network connections—specifically, those that gave rise to the successful (rewarded) behavior. Thus, post-performance beta oscillations would serve to increase the likelihood that the rewarded outcome would be obtained in similar situations in the future.

In this regard, our findings may indicate a causal relation between the abnormally high beta synchrony in the cortex[27,28] and basal ganglia[29,30] of PD patients and a specific type of learning deficit associated with PD. A recent study[31] found that PD patients were more likely than normal subjects to perseverate in their choices, independently of reward

history, and that this perseveration in choice decreased with dopaminergic therapy. Notably, beta activity in PD patients has also been shown to decrease with dopaminergic treatment. Given the increased beta bursting we found in CN and dlPFC following correct trials relative to error trials, we propose that the persistently (and indiscriminately) high beta activity in PD patients could drive their future choices by reinforcing the behavior that led to the previous choice, regardless of whether it was rewarded. Alternatively, the high beta activity might prevent the plasticity necessary for the brain to learn from an erroneous choice, modify the network settings accordingly, and increase the likelihood of choosing correctly in future trials. Either way, the high beta synchrony associated with PD could help explain the abnormal choice perseveration observed in these patients. We predict that the direct manipulation of beta activity in PD patients might bestow cognitive benefits (in the form of a decrease in the perseveration of choice errors), in addition to the known motor benefits (reduced akinesia).

We were particularly struck by the unique features of beta activity in the dlPFC. Despite the fact that across all tasks the dlPFC had the lowest rate of bursts among the four studied brain regions, during the post-trial period it exhibited the greatest change in burst rates relative to rest (Figs. 1b & 3a). Furthermore, the dlPFC alone exhibited modulation of post-trial burst rates by both the number of visual cues and by the number of movements in the preceding trial. The greater the number of visual stimuli, and the greater the number of the responses the monkey made to them, the higher the post-performance burst rates were in dlPFC. Thus it appears that dlPFC bursts in the post-trial period were tracking the cognitive load during the preceding trial. Furthermore, the preliminary results of our population-wide burst co-activation analysis indicate that not

only were prefrontal burst rates in the post-trial period more spatially localized than they were in the other brain regions, but these bursts became increasingly more localized with increasing cognitive load during the preceding trial, even though the burst rates increased. This stood in contrast to the results from the other three brain regions, in which post-trial burst rates and the level of within-structure co-activation went hand-in-hand. Taken together, these results are consistent with the accepted role of dlPFC in executive control[22], and support our view of the involvement of beta activity in the post-performance coordination of neural activity across multiple sites in the brain.

METHODS

Recording methods

All methods were approved by the MIT Committee on Animal Care and accord with the NIH guidelines for the use of laboratory animals. Procedures were performed under sterile conditions on anesthetized monkeys placed in a standard stereotaxic apparatus. A titanium headpost and Delrin recording chamber was implanted and subsequent procedures were performed to enlarge craniotomies and thin the dura mater and granulation tissue. Using a custom-built plastic grid with precisely machined holes (1 mm center-to-center), we recorded LFP activity from cortical and sub-cortical structures accessible through a large (1600 mm^2) bilateral craniotomy over the frontal lobes. Recordings were obtained from up to 128 electrodes implanted in up to ~14 structures bilaterally, including prefrontal cortex, primary and premotor cortex, supplementary motor areas, cingulate cortex and striatum. By adjusting the depth of each electrode (upward or downward) over the course of an implant, we recorded from sites at multiple depths along each track. Implants were removable and reconfigurable, enabling us to target different regions or different tracks within the same region from one implant to the next. We collected neural data during ~60 sessions per monkey, across 2-3 implants, in order to have sufficient data to analyze from multiple recording sites.

Behavioral Tasks

The monkeys were placed on a food- or water-restricted diet, in accordance with the MIT CAC protocol. They were trained on a set of novel joystick tasks to perform internally timed, visually guided arm movements, in response to visual cues, in order to receive

liquefied reward (delivered by a computer-controlled pump). In each recording session the monkey sat comfortably in a purpose-built chair inside a sound-attenuated recording booth (Crist Instruments, MD). A rigid plastic bar connected the monkey's head-post to the chair frame. A second bar was used to stabilize the recording chamber, as needed. The monkey's left (unused) arm was lightly restrained to the chair. Its right arm was free to grasp an analog joystick (modified from Happ Controls, Inc., 10.5 cm long with a 1.9 cm diameter), which, upon deflection, exerted a mild restoring force toward the center position. The joystick was fixed to the inner wall of the recording booth beneath the display screen (30 cm from the monkey's waist). The joystick was calibrated so that a 1 cm deflection corresponded to a 2 cm displacement of the cursor on the screen, and was restricted to move in only 8 directions by a horizontal plate with 8 tracks cut into it in a star-shaped pattern. The trials of the different tasks were presented in separate blocks, according to a fixed schedule. The trials in each block were presented pseudo-randomly until the monkey correctly completed all of them.

To initiate a new trial, the monkey had to touch and hold the joystick steady at the center position, upon which an array of 8 "empty" (colorless with red outline) circular peripheral cues (4° visual angle) appeared equidistantly (9° visual angle) from the empty center cue (5° visual angle). The appearance of the empty cue array marked the start of a variable center hold period, which lasted for 0.5-1 s. At the end of this variable-duration period, the empty center cue was filled with yellow and, depending on the task, 1 or 3 of the 8 peripheral cues were each filled with a different color (red, green and blue, or purple, aqua and orange, depending on the block of trials). Each cue could be filled with color in the shape of a solid disc or an annulus with a black center. The simultaneous

onset of the cues marked the beginning of the first self-timed center hold interval, at the end of which the monkey had to initiate a joystick movement (except in trials of the **0M3T** task, as described below). The locations of the peripheral cues encoded the required joystick movement targets. Importantly, other than the appearance of the colored cues at the start of the first self-timed center hold interval, no external cues were presented to trigger the monkey's arm movement(s). The monkey had to self-time the duration of the first center hold interval, as indicated by the shape of the center yellow cue (solid disc: 0.6-1.2 s or "short"; annulus: 1.4-2.0 s or "long"). Even in sequential movement trials (with multiple arm movements), the monkey had to self-time the initiation of each arm movement in the sequence. This novel feature of the behavioral tasks was designed to enable the detection of internally generated oscillations that are not direct (evoked) responses to changes in the environment.

In sequential movement trials, the colors of the cues indicated the order of the movements to be performed. The color-order codes were fixed across all recording sessions. Thus, the locations of the red (purple), green (aqua) and blue (orange) cues always indicated the first, second and third movement directions, respectively. The solid or annular shape of the peripheral cue related to the most recently completed movement indicated the required duration of the subsequent center hold interval.

Upon successful completion of a trial, reward was delivered (~0.3 s), followed by the post-trial period (~3 s). If at any point in the trial the monkey failed one of the requirements (e.g., began moving the joystick too early, or did not move it in the correct direction), the trial was immediately aborted.

At the start and end of each recording session, we collected data during prolonged rest periods with the head-fixed monkey sitting quietly inside or outside of the recording booth. In each recording session, the monkey performed blocks of trials of the following tasks:

The **1M1T** task required the monkey to perform a single center-out-center joystick movement in response to a single peripheral cue, following a short or long self-timed hold period. After performing the single movement, the monkey had to continue to hold the joystick at the center position for a pre-reward interval of variable duration (1.2-2.6 s). Each block of the single movement was comprised of 64 trials – two copies each of all possible combinations of spatial movement direction and pre- and post-movement hold interval durations.

The **3M3T** task required the monkey to perform sequences of three joystick movements, each preceded by a short or long self-timed center hold period, with reward delivered only following the final movement. All of the cues for the entire sequence appeared simultaneously at trial-start and remained unchanged on the screen for the duration of the trial. Thus, the monkey could collect the visual information it needed to perform the entire arm movement sequence prior to initiating any part of it. Moreover, the monkey had to proceed from one sequential movement to the next without the benefit of suddenly appearing cues, relying instead of internal guidance to execute the entire sequence of self-timed arm movements.

In each block of the **3M3T** task the monkey had to correctly complete 32 trials, each requiring a distinct spatiotemporal sequence of joystick movements. Each sequence could be broken down conceptually into spatial and temporal templates. There were eight

possible temporal templates (*short*, *short*, *short*; *short*, *short*, *long*; *short*, *long*, *short*; etc.) and 8 x 7 x 6 = 336 spatial templates. At the start of each recording session, a unique set of 32 sequences to be used that day was constructed according to a prescription that ensured that each of the eight temporal templates occurred exactly four times in each block of trials. Since the monkeys had been trained extensively on all combinations of spatial and temporal templates prior to the recording phase of the experiment, we expected little learning to occur within any given recording session.

The **1M3T** task was visually identical to the **3M3T** task, but the monkey had to perform only the first of the three cued center-out-center joystick movements. In this task, the green and blue (or aqua and orange) cues served essentially as distractors. In order to receive reward following the single joystick movement, the monkey had to continue to hold at the center position for a variable period of time that was substantially longer than the maximum time that it would have been allowed to wait before initiating the next sequential movement in an ordinary **3M3T** trial. By forcing the monkey to wait for an extended period of time, we could rule out the possibility that it was preparing to perform the sequence (correctly), rather than the single movement alone.

The **0M3T** task was also visually identical to the **3M3T** task, but the monkey had to withhold all joystick movement in order to receive reward. Following the appearance of the cues, the monkey had to continue holding the joystick at the center position for a variable period of time that was substantially greater than what it would have been allowed to wait before initiating the first movement in a visually identical **3M3T** trial.

Data Acquisition

Neuronal signals were amplified and filtered (600-6000 Hz for spikes, and 1-475 Hz for LFPs) by a Cheetah acquisition system (Neuralynx, Bozeman, MT). Spike waveforms (32 kHz sampling rate) and LFP signals (2 kHz) were continuously collected during daily recording sessions. The Cheetah system was configured to accommodate up to 128 single electrodes along with eight analog input channels (for behavioral data). At the start of each recording session, we used custom-made software to configure each electrode channel to record either spike or LFP data. In addition, we recorded both spike and LFP signals simultaneously from up to 24 electrodes that were selected daily. Each neural (spike or LFP) data channel was stored to a separate file. Spike data was not analyzed for this thesis. Neural data was monitored online, during recordings, using headphones and online-cluster-cutting and visualization tools (NEX, Plexon and Cheetah, Neurlaynx) for spikes, and scrolling visual displays for LFPs. Eye position, blinks and pupil size were recorded by the infra-red camera-based Eyelink II system (500 Hz, SR Research, Canada), and a touch-monitor (100 Hz) was used to detect joystick touching. Joystick position (200 Hz), eye position and the touch-sensor were monitored by a computer running custom-written code in Delphi (visual Pascal) to control the experiment. All behavioral data and task events were sent to the Cheetah system for time-stamping and storage along with the neural signals. A video camera mounted inside the recording booth was used to monitor the space surrounding the joystick, and the images (30 Hz) were time-stamped by Cheetah and stored.

Histology

After the experiments are completed, each monkey was perfused intracardially with fixative (0.9% NaCl followed by 4% paraformaldehyde in 0.01 M Na^{2+}/K^{-} PO_4 buffer, pH 7.4), before removing the final chronic implant. Several electrolytic lesions (10 μA DC for 10 s, < 15 sites) were made to mark locations in the brain relative to the grid. Conventional Nissl staining (60 μm thick slices) was performed to visualize electrode tracks. The slices were analyzed to reconstruct the location of each electrode in each recording session. Tracks from earlier chronic implants were reconstructed on the assumption that the distance from the grid to the surface of the brain was constant across implants.

Data Analysis

In order to assess the role of beta activity in movement behavior, we designed a set of movement tasks that together could be used to tease apart cognitive features of behavior from the details of motor execution. The following methods were used to characterize the time-course of beta activity at each recording site and to compare and contrast this activity (1) across tasks for each site, and (2) across sites for each task:

1. Trial-Averaged LFP Power We used open-source Chronux algorithms (http://chronux.org), in-house software, Matlab (MathWorks, MA) Toolboxes, and other libraries. We estimated frequency spectra using the multitaper method, by adjusting the time window, the number of tapers and time-bandwidth product of the tapers to suit the LFP signals being studied. Power spectra for each taper and each trial were averaged over tapers and trials. To make spectrograms, a raw waveform was divided into a series of overlapping time windows of equal size, and spectral power in each window was

displayed according to a color scale in a vertical strip at the center of the time window. The DC component and event-aligned evoked potential were removed, and the raw waveforms was padded at the end with zeros to produce a finer frequency grid. Band-limited spectral power within peri-event periods was calculated first by computing a single-taper (Hamming window) unpadded spectrogram for each trial and for each electrode. We used a 1 s window moving in 0.04 s steps across trial-time for frequency below 30 Hz, a 0.3 s window moving in 0.02 s steps for the 20-60 Hz band, and narrower windows of width at least equal to four cycles of the lowest frequency in higher frequency bands. The power components were summed for the frequency band between its upper and lower limits and the time series was linearly interpolated at the sample rate used for acquisition of LFP activity (2 KHz). The trial-averaged power in the beta band was aligned on each behavioral event and 95% confidence intervals were computed and used to detect peri-event periods of significant modulation. The results were compared across brain areas and tasks. Statistical significance will be assessed using the Mann-Whitney test for differences in beta power at each time point in a 500 ms-window around each task event or the ANOVA, corrected for multiple comparisons (alpha = 0.05).

2. Single-Trial LFP Power Beta power in our experiments was characterized by brief bursts of varying amplitude, which cannot be detected in the trial averaged power spectrograms. To study the time-course of beta activity in individual trials, we adapted the Hilbert-Huang transform method to make it applicable to our LFP data. This allowed us to analyze the bursts in beta power on single trials without the temporal smoothing required by Fourier-based methods or the ringing caused by band-pass filters. We studied the timing of bursts relative to behavioral events, and the rates of bursts in each of 4 trial

epochs (defined in the legend of **Fig. 1**). Burst rate and amplitude measures were studied raw and also normalized to the average values during rest periods (separately for each recording site). Differences in burst measures across epochs and brain regions were assessed using the ANOVA corrected for multiple comparisons (alpha = 0.05).

3. LFP-LFP Coherence The magnitude and phase of the coherence among LFPs recorded simultaneously at pairs of sites (within and among brain structures) were calculated during the post-trial period. To calculate LFP-LFP coherence, we computed the FFTs of the tapered waveforms individually for each taper and each trial. Cross-spectra computed from the individual FFTs were averaged over tapers and trials. Coherence was then computed as $C = S_{12} / sqrt(S_1 * S_2)$, where S_{12} denotes the averaged cross-spectrum and S_1 and S_2 denote the averaged power spectra of the two signals. Coherence phase was calculated in time-and-frequency windows with statistically significant coherence ($p < 0.01$, *t*-test). For coherence magnitude, 95% confidence limits were computed using a jackknife procedure. For coherence phase, confidence limits were estimated by the formula: $mean \pm 2 * sqrt((1 / K * Ntr) * (1 / (C\^2) - 1))$, where *mean* is the mean coherence phase at a given frequency, K is the number of tapers, Ntr is the number of trials, and C is the coherence magnitude at that frequency. To verify that coherence results were due to time-locked dependencies between the two signals and not to a time-independent regularity, analyses yielding significant results were repeated after shuffling the order of trials for one signal but not the other, producing an estimate of the expected false-positive rate, for all coherence, spike-triggered averaging and phase histograms.

REFERENCES

1 Neuper, C., Wortz, M. & Pfurtscheller, G. ERD/ERS patterns reflecting sensorimotor activation and deactivation. *Prog Brain Res* **159**, 211-222, doi:10.1016/S0079-6123(06)59014-4 (2006).

2 Stancak, A., Jr. & Pfurtscheller, G. Event-related desynchronisation of central beta-rhythms during brisk and slow self-paced finger movements of dominant and nondominant hand. *Brain Res Cogn Brain Res* **4**, 171-183 (1996).

3 Sanes, J. N. & Donoghue, J. P. Oscillations in local field potentials of the primate motor cortex during voluntary movement. *Proc Natl Acad Sci U S A* **90**, 4470-4474 (1993).

4 Rubino, D., Robbins, K. A. & Hatsopoulos, N. G. Propagating waves mediate information transfer in the motor cortex. *Nat Neurosci* **9**, 1549-1557, doi:10.1038/nn1802 (2006).

5 Pfurtscheller, G., Stancak, A., Jr. & Neuper, C. Post-movement beta synchronization. A correlate of an idling motor area? *Electroencephalogr Clin Neurophysiol* **98**, 281-293 (1996).

6 Hammond, C., Bergman, H. & Brown, P. Pathological synchronization in Parkinson's disease: networks, models and treatments. *Trends Neurosci* **30**, 357-364, doi:10.1016/j.tins.2007.05.004 (2007).

7 Brown, P. *et al.* Effects of stimulation of the subthalamic area on oscillatory pallidal activity in Parkinson's disease. *Exp Neurol* **188**, 480-490, doi:10.1016/j.expneurol.2004.05.009 (2004).

8 Alonso-Frech, F. *et al.* Slow oscillatory activity and levodopa-induced dyskinesias in Parkinson's disease. *Brain* **129**, 1748-1757, doi:10.1093/brain/awl103 (2006).

9 Kuhn, A. A. *et al.* High-frequency stimulation of the subthalamic nucleus suppresses oscillatory beta activity in patients with Parkinson's disease in parallel with improvement in motor performance. *J Neurosci* **28**, 6165-6173, doi:10.1523/JNEUROSCI.0282-08.2008 (2008).

10 Pogosyan, A., Gaynor, L. D., Eusebio, A. & Brown, P. Boosting cortical activity at Beta-band frequencies slows movement in humans. *Curr Biol* **19**, 1637-1641, doi:10.1016/j.cub.2009.07.074 (2009).

11 Lozano, A. M., Dostrovsky, J., Chen, R. & Ashby, P. Deep brain stimulation for Parkinson's disease: disrupting the disruption. *Lancet Neurol* **1**, 225-231 (2002).

12 Owen, A. M. *et al.* Fronto-striatal cognitive deficits at different stages of Parkinson's disease. *Brain* **115 (Pt 6)**, 1727-1751 (1992).

13 Swainson, R. *et al.* Probabilistic learning and reversal deficits in patients with Parkinson's disease or frontal or temporal lobe lesions: possible adverse effects of dopaminergic medication. *Neuropsychologia* **38**, 596-612 (2000).

14 Brown, P. & Williams, D. Basal ganglia local field potential activity: character and functional significance in the human. *Clin Neurophysiol* **116**, 2510-2519, doi:10.1016/j.clinph.2005.05.009 (2005).

15 Baker, S. N., Olivier, E. & Lemon, R. N. Coherent oscillations in monkey motor cortex and hand muscle EMG show task-dependent modulation. *J Physiol* **501 (Pt 1)**, 225-241 (1997).

16 Androulidakis, A. G. *et al.* Anticipatory changes in beta synchrony in the human corticospinal system and associated improvements in task performance. *Eur J Neurosci* **25**, 3758-3765, doi:10.1111/j.1460-9568.2007.05620.x (2007).

17 Gilbertson, T. *et al.* Existing motor state is favored at the expense of new movement during 13-35 Hz oscillatory synchrony in the human corticospinal system. *J Neurosci* **25**, 7771-7779, doi:10.1523/JNEUROSCI.1762-05.2005 (2005).

18 Engel, A. K. & Fries, P. Beta-band oscillations--signalling the status quo? *Curr Opin Neurobiol* **20**, 156-165, doi:10.1016/j.conb.2010.02.015 (2010).

19 Saint-Cyr, J. A. Frontal-striatal circuit functions: context, sequence, and consequence. *J Int Neuropsychol Soc* **9**, 103-127 (2003).

20 Kermadi, I. & Joseph, J. P. Activity in the caudate nucleus of monkey during spatial sequencing. *J Neurophysiol* **74**, 911-933 (1995).

21 Barone, P. & Joseph, J. P. Prefrontal cortex and spatial sequencing in macaque monkey. *Exp Brain Res* **78**, 447-464 (1989).

22 Miller, E. K. & Cohen, J. D. An integrative theory of prefrontal cortex function. *Annu Rev Neurosci* **24**, 167-202, doi:10.1146/annurev.neuro.24.1.167 (2001).

23 Kopell, N., Ermentrout, G. B., Whittington, M. A. & Traub, R. D. Gamma rhythms and beta rhythms have different synchronization properties. *Proc Natl Acad Sci U S A* **97**, 1867-1872 (2000).

24 Pesaran, B., Nelson, M. J. & Andersen, R. A. Free choice activates a decision circuit between frontal and parietal cortex. *Nature* **453**, 406-409, doi:10.1038/nature06849 (2008).

25 Tsai, T. Y. *et al.* Robust, tunable biological oscillations from interlinked positive and negative feedback loops. *Science* **321**, 126-129, doi:10.1126/science.1156951 (2008).

26 Holgado, A. J., Terry, J. R. & Bogacz, R. Conditions for the generation of beta oscillations in the subthalamic nucleus-globus pallidus network. *J Neurosci* **30**, 12340-12352, doi:10.1523/JNEUROSCI.0817-10.2010 (2010).

27 Marsden, J. F., Limousin-Dowsey, P., Ashby, P., Pollak, P. & Brown, P. Subthalamic nucleus, sensorimotor cortex and muscle interrelationships in Parkinson's disease. *Brain* **124**, 378-388 (2001).

28 Williams, D. *et al.* Dopamine-dependent changes in the functional connectivity between basal ganglia and cerebral cortex in humans. *Brain* **125**, 1558-1569 (2002).

29 Brown, P. *et al.* Dopamine dependency of oscillations between subthalamic nucleus and pallidum in Parkinson's disease. *J Neurosci* **21**, 1033-1038 (2001).

30 Cassidy, M. *et al.* Movement-related changes in synchronization in the human basal ganglia. *Brain* **125**, 1235-1246 (2002).

31 Rutledge, R. B. *et al.* Dopaminergic drugs modulate learning rates and perseveration in Parkinson's patients in a dynamic foraging task. *J Neurosci* **29**, 15104-15114, doi:10.1523/JNEUROSCI.3524-09.2009 (2009).

FIGURE LEGENDS

Figure 1 | Suppression-rebound pattern of the task-modulation of beta power across simultaneously recorded LFPs in M1PMC, dlPFC, CN and Put. (a) Schematic flow of trials of the single (1M1T) or sequential (3M3T) self-timed joystick movement tasks. Timelines show the division of each trial into contiguous periods for analysis (top): Cue – from onset of empty cue array until the initiation of joystick movement; Movement – from initiation to joystick movement until 700 ms following the offset of the last movement; Post-movement – from the end of the movement period until the offset of the visual cues (following reward delivery); and Post-trial – from the offset of the visual cues until the start of the next trial (3 s). Each movement was preceded by a short (0.8 s) or long (1.6 s) duration hold period that the monkeys had to self-time. Trials of each task were presented in separate blocks in each experimental session. Following the last movement in a trial, the monkeys held the joystick steady for a variable delay until reward delivery, immediately after which the visual cues disappeared and a 3 s-long post-trial period began. The spatial locations, shapes and colors of the cues, indicated the movement targets, durations of pre-movement hold periods and order of movements, and were changed pseudorandomly from trial-to-trial. Trials of every combination of short and long hold periods were performed in each session. (b) Bandpass-filtered LFP power in the beta band recorded from each electrode was averaged across all correct trials of the short (top left) and long (bottom left) 1M1T tasks, and the short-short-short (top right) and long-long-long (bottom right) 3M3T tasks performed in a single session. The power for each site was then normalized to the average rest value at that site. Results were averaged across the population of LFPs recorded in each brain region in four sessions and

plotted in ten time-windows centered on successive task events (C – onset of the array of visual cues, 1-3 – joystick movements, Rwd – reward delivery; pairs of colored traces indicate upper and lower 95% confidence limits), shown together as a single composite figure.

Figure 2 | Bursts of beta oscillations in M1PMC, dlPFC, CN and Put. (a) The beta band content of the Hilbert-Huang transform (HHT) of an LFP recorded in a single 1M1T trial (top, red) exhibited short episodes during which it accounted for a relatively large fraction of the spectrum of the raw LFP (bottom, black arrows). The beta bandpass-filtered waveform (bottom, blue) showed similar modulation to the HHT, but with considerably less accuracy (in terms of faithful representation of beta oscillations in the raw LFP). (b) Beta bursts varied in amplitude and timing across correct trials of the short-short-short and long-long-long 3M3T task in three simultaneously recorded LFPs in M1PMC, dlPFC and CN. The rate of beta bursts at each site varied systematically in relation to task events, following a similar time-course to that of the trial-averaged beta power at the same site. Trials began at time 0. Vertical lines indicate task events (yellow – onset of visual cues, red, green and blue – 1^{st}-3^{rd} joystick movements, magenta – reward delivery, grey – start of next trial). (c) The maximum cross-covariance between the envelopes of beta bursts recorded at pairs of sites was averaged across all pairs within each brain region (thick lines - means; shading – 95% confidence limits). For inter-electrode distances of < 1.5 mm the values of the cross-covariance were not significantly different across brain regions. However, at greater distances, the average values for dlPFC pairs fell more quickly than the values for the other brain regions.

Figure 3 | Differential modulation of population beta burst rates in M1PMC, dlPFC, CN and Put by behavioral tasks. (a) The beta burst rate for each LFP in each task and task period was averaged across trials. The resulting burst rates for each LFP were normalized by the average value during rest periods for that LFP, and then the burst rates were averaged across the population of LFPs recorded in each brain region, across all sessions (horizontal dashed line denotes population average burst rate during rest periods). The population-average of normalized burst rates in each brain region followed a pattern of modulation that was similar to the time-course of beta band power in that region. There were no data points for the movement and post-movement periods in the 0M3T task. (b-e) Population average normalized burst rates shown in each brain region across tasks during post-trial periods following correct and error trials (thick solid and thin dashed lines, respectively; shading – 95% confidence limits). The values for correct trials were re-plotted from right-most plot in (a) with different vertical scales. Asterisks indicate statistically significant differences between adjacent pairs of data points in correct trials or separately in error trials (ANOVA corrected for multiple comparisons, alpha = 0.05). Statistically significant differences between correct and error trials are demonstrated by non-overlapping shading (95% confidence intervals) between the thick and thin lines.

Figure 4 | Beta range coherence between dlPFC and CN is highest in the post-trial period and disproportionately due to bursts. (a) Population average coherograms across all pairs of simultaneously recorded LFPs in dlPFC and CN across all sessions. Coherence magnitude is shown in pseudocolor across correct trials of the short 1M1T and short-

short-short 3M3T tasks. The values, shown in windows aligned on the task events, indicate a significant peak in the beta band (~15 Hz) during the post-trial period. (b) Example from a single pair of CN-dlPFC LFPs, showing increased coherence in the post-trial period when both LFPs are bursting, as opposed to when neither is bursting (top plot; thick lines – means, shading – 95% confidence limits). The phase of the beta band coherence in both cases was significantly lower than zero (bottom plot). The striatal LFP led the prefrontal one by ~ 8 ms. (c) Same as (a) for long 1M1T and long-long-long 3M3T tasks. (d) Same as (b) for all post-trial periods following correct trials of the 3M3T task.

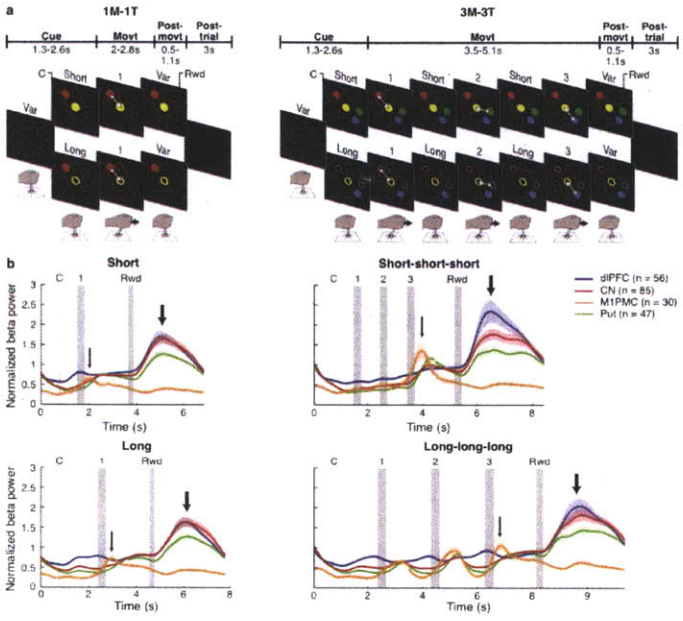
a
1M-1T
Cue
1.3-2.6s
Movt
2-2.6s
Post-movt
0.5-1.1s
Post-trial
3s
C
Short
1
Var
Rwd
Var
Long
1
Var
3M-3T
Cue
1.3-2.6s
Movt
3.5-5.1s
Post-movt
0.5-1.1s
Post-trial
3s
C
Short
1
Short
2
Short
3
Var
Rwd
Var
Long
1
Long
2
Long
3
Var
b
Short
Short-short-short
Long
Long-long-long
C
1
2
3
Rwd
Normalized beta power
Time (s)
dlPFC (n = 56)
CN (n = 85)
M1PMC (n = 30)
Put (n = 47)

Figure 1

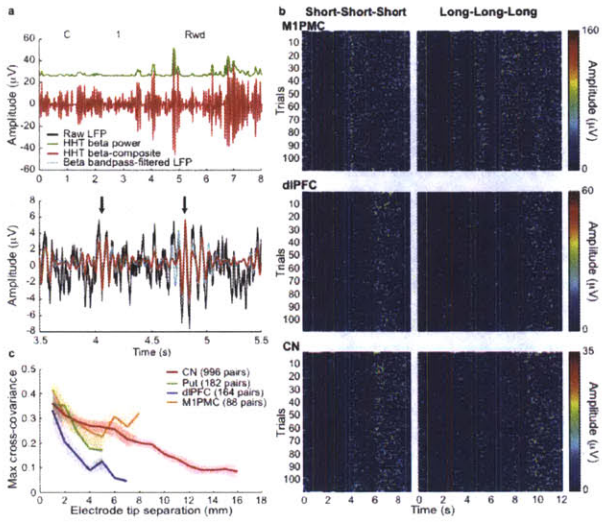
a
C
1
Rwd
Amplitude (μV)
Raw LFP
HHT beta power
HHT beta-composite
Beta bandpass-filtered LFP
Time (s)
b
Short-Short-Short
Long-Long-Long
M1PMC
dlPFC
CN
Trials
Amplitude (μV)
Time (s)
c
Max cross-covariance
CN (996 pairs)
Put (182 pairs)
dlPFC (164 pairs)
M1PMC (86 pairs)
Electrode tip separation (mm)

Figure 2

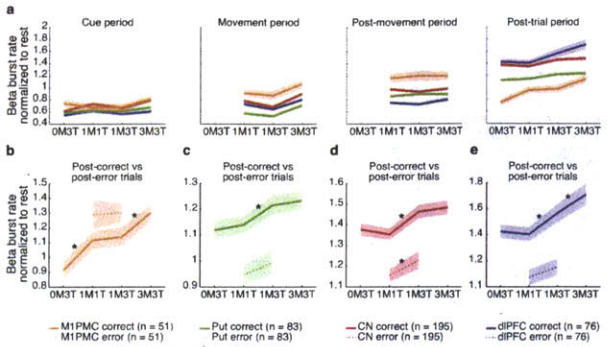
a
Cue period
Movement period
Post-movement period
Post-trial period
Beta burst rate normalized to rest
0M3T 1M1T 1M3T 3M3T
b
c
d
e
Post-correct vs post-error trials
M1PMC correct (n = 51)
M1PMC error (n = 51)
Put correct (n = 83)
Put error (n = 83)
CN correct (n = 195)
CN error (n = 195)
dlPFC correct (n = 76)
dlPFC error (n = 76)

Figure 3

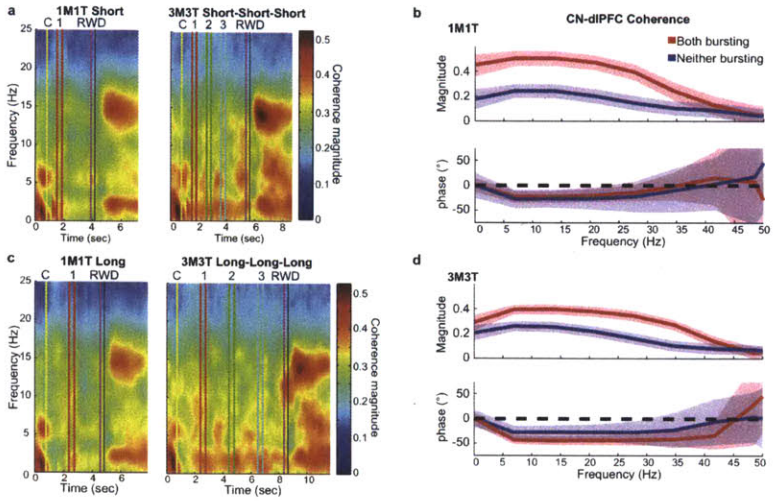
a
1M1T Short
C 1 RWD
3M3T Short-Short-Short
C 1 2 3 RWD
Frequency (Hz)
Time (sec)
Coherence magnitude
b
CN-dlPFC Coherence
1M1T
Both bursting
Neither bursting
Magnitude
phase (°)
Frequency (Hz)
c
1M1T Long
C 1 RWD
3M3T Long-Long-Long
C 1 2 3 RWD
d
3M3T

Figure 4

SUPPLEMENTARY FIGURE LEGENDS

Supplementary Figure 1 | Suppression-rebound pattern of the task-modulation of beta power across individual simultaneously recorded LFPs in M1PMC, dlPFC, CN and Put. Each row shows the bandpass-filtered LFP power in the beta band recorded from a single site in a given brain region, averaged across all correct trials of the short 0M3T, 1M1T, 1M3T and 3M3T tasks in a single session (shading – 95% confidence limits). The LFPs were simultaneously recorded. The trial-averaged beta power follows a suppression-rebound modulation pattern resembling the population averages (Fig. 1b), and even in the absence of arm movement (0M3T). Interestingly, differences can be observed between the maxima in average beta power at a given site across tasks. These differences are quantitatively analyzed in terms of burst rates (Fig. 3) and power (Supplementary Fig. 4).

Supplementary Figure 2 | Single trial examples of beta burst activity across simultaneously recorded sites in M1PMC, dlPFC, CN and Put. The rates of bursts in single trials of the short-short-short and long-long-long 3M3T tasks (left and right, respectively) are differentially modulated by task events in different brain regions. Bursts across sites in M1PMC occur predominantly following movement, whereas in the other brain regions, they occur mostly during the Post-trial period. Beta bursts across sites in the striatum appear to be dramatically coincident, especially compared to the bursts across prefrontal sites. This difference in the within-region co-activation of bursts between striatum and dlPFC was reflected in the cross-covariance analysis (Fig. 2c) and the co-activation analysis described in the text.

Supplementary Figure 3 | The coherence between beta bursts recorded simultaneously between the closest pair of sites in the CN had significantly non-zero phase in the beta range (blue traces – upper and lower 95% confidence limits).

Supplementary Figure 4 | Beta bursts are modulated by tasks and task epochs. (a) As in Fig. 3a but for population average normalized burst power, as opposed to rate. (b) As in Fig. 3a but for the population average of actual burst rates (i.e., not normalized to rest). The burst rates in dlPFC were consistently lowest across epochs and tasks, even though the normalized rates in dlPFC, shown in (a), reached the highest values among all brain regions. (c-f) Examples of the rest-normalized burst rates of individual LFPs in the Post-trial period shown in thin colored lines (solid – Monkey 1, dashed – Monkey 2; shading – 95% confidence limits) exhibited similar across-task modulation as the population averages (thick lines, replotted from Fig. 3c-f).

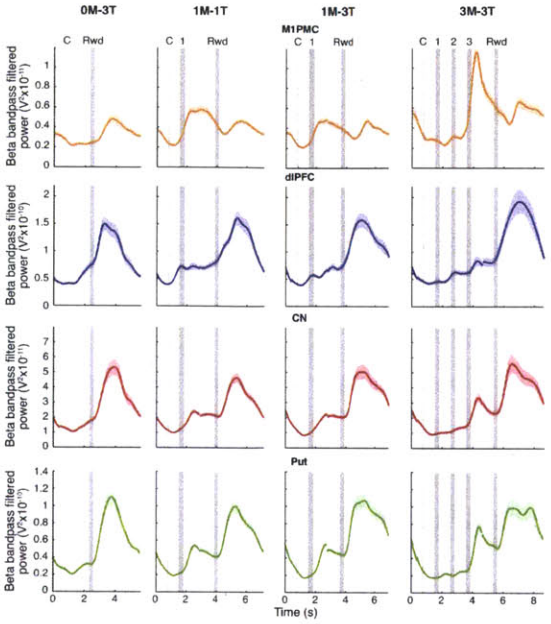

Supplementary Figure 1

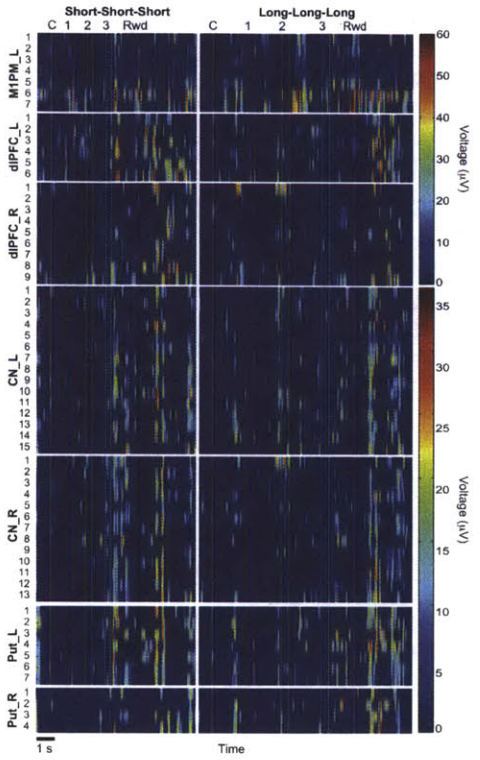

Supplementary Figure 2

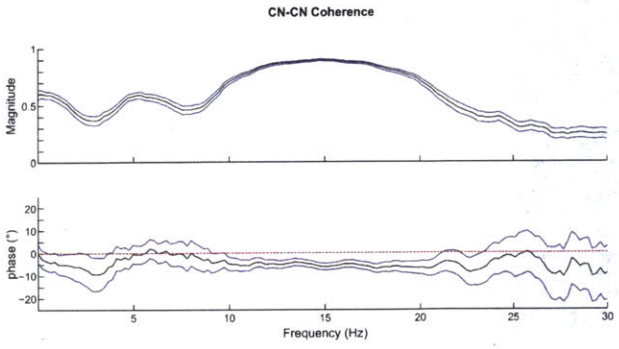

Supplementary Figure 3

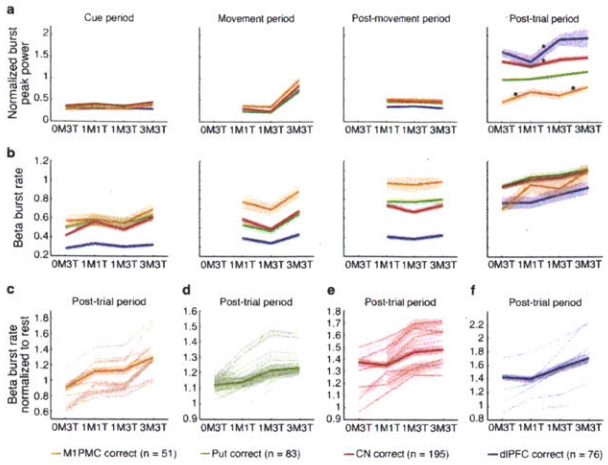

Supplementary Figure 4